

# Thermodynamic Evolution of Secluded Vector Dark Matter: Conventional WIMPs and Nonconventional WIMPs

Kwei-Chou Yang<sup>1,\*</sup>

<sup>1</sup>*Department of Physics and Center for High Energy Physics,  
Chung Yuan Christian University, Taoyuan 320, Taiwan*

The secluded dark matter resides within a hidden sector and self-annihilates into lighter mediators which subsequently decay to the Standard Model (SM) particles. Depending on the coupling strength of the mediator to the SM, the hidden sector can be kinetically decoupled from the SM bath when the temperature drops below the mediator's mass, and the dark matter annihilation cross section at freeze-out is thus possible to be boosted above the conventional value of weak interacting massive particles. We present a comprehensive study on thermodynamic evolution of the hidden sector from the first principle, using the simplest secluded vector dark matter model. Motivated by the observation of Galactic center gamma-ray excess, we take two mass sets  $\sim \mathcal{O}(80 \text{ GeV})$  for the dark matter and mediator as examples to illustrate the thermodynamics. The coupled Boltzmann moment equations for number densities and temperature evolutions of the hidden sector are numerically solved. The formalism can be easily extended to a general secluded dark matter model. We show that a long-lived mediator can result in a boosted dark matter annihilation cross section to account for the relic abundance. We further show the parameter space which provides a good fit to the Galactic center excess data and is compatible with the current bounds and LUX-ZEPLIN projected sensitivity. We find that the future observations of dwarf spheroidal galaxies offer promising reach to probe the most relic allowed parameter space relevant to the boosted dark matter annihilation cross section.

---

\* [kcyang@cycu.edu.tw](mailto:kcyang@cycu.edu.tw)

## I. INTRODUCTION

Motivated by particle physics, the theoretical studies and experimental searches have for many decades focused on the popular class of the dark matter (DM) candidates, called the weakly interacting massive particles (WIMPs). In the WIMP scenario, when the dark matter becomes nonrelativistic, its comoving number density is exponentially depleted through Boltzmann suppression and keeps the thermal equilibrium with the bath until freeze-out. The resulting DM with the weak scale interaction and mass can provide the correct relic abundance today.

Many DM experiments are thus motivated by the WIMP scenario. Nevertheless, no conclusive observations have been made by the direct detection searches, Large Hadron Collider (LHC), and other collider experiments. Several groups have reported the GeV gamma-ray excess around the Galactic center (GC) [1–11], for which, however, the allowed WIMP dark matter models have been also severely constrained by the current null results of the direct detection [12–15] and collider experiments. In light of these measurements, an interesting paradigm that goes beyond the “conventional” WIMP scenario and becomes more and more popular is known as “secluded (WIMP) dark matter”. In this paradigm, the dark matter candidate may reside within one of the hidden sectors and communicates with the visible sector through a lighter metastable mediator, which weakly couples the standard model (SM) to the WIMP. As such, the DM signals, suppressed at the direct detection and colliders, could be observable in indirect measurements [16–25].

The mechanism for the secluded WIMP dark matter was discussed by Pospelov, Ritz, and Voloshin [16]. In this mechanism, the WIMP can still be a thermal relic, and the dominant DM annihilation channel is into a pair of unstable mediators which ultimately decay into SM particles. Basically, for this model, as long as the mediator decays before the beginning of the big bang nucleosynthesis (BBN), the effective number of neutrino species and abundance of helium and deuterium will not be modified, as compared with the standard BBN, so that the result can be easily compatible with the current Planck measurement [26].

As for building secluded DM models, many people restricted their works to the parameter space relevant to the WIMP scenario where the hidden sector is in chemical and thermal equilibrium with the bath prior to freeze-out [17–24]. However, for the case that the dark sector has kinetically decoupled from the bath, due to its weak couplings to the SM particles, before it becomes nonrelativistic, if the secluded DM annihilates into nearly degenerate mediators which later decay out-of-equilibrium with the bath, the DM density will be exponentially depleted through the decay process of the mediator, instead of following Boltzmann suppression [27]. Moreover, during the

period of time in which the dark sector is out of thermal equilibrium with the bath, if the  $3 \rightarrow 2$  number changing interactions are allowed and efficiently active, the hidden sector can first undergo an epoch called “cannibalism”. See the related discussions in Refs. [28–31]. Alternatively,  $3 \rightarrow 2$  DM annihilation mechanism is also relevant to the strongly-interacting massive particles (or called SIMP) [32] and elastically decoupling relic (or called ELDER) [33, 34] scenarios.

In this paper, to have a thorough understanding about the thermodynamics of the secluded dark matter from the first principle, we will study the simplest secluded vector dark matter model, taken as an example in which the vector dark matter and the mediator within the hidden sector are in thermal equilibrium with each other before freeze-out, but may be kinetically decoupled from the SM bath at temperature  $T \sim m_{X,S}$ , depending on the couplings to the SM, where  $m_X$  and  $m_S$  are the masses of the DM and hidden scalar, respectively.

We separately obtain the evolution equations of number densities and temperatures for the hidden species, by taking suitable moments of the Boltzmann equation. We will give a detailed result of describing chemical and kinetic decouplings of the hidden sector from the thermal bath. We will show that, depending on the coupling strength of the mediator to the SM, the relic annihilation cross section is likely to be boosted above the conventional WIMP value. The present study can be easily generalized to a generic case.

Using two mass sets: (i)  $m_X = 80$  GeV,  $m_S = 0.8m_X$ , and (ii)  $m_X = 80$  GeV,  $m_S = 0.99m_X$ , we numerically solve the thermodynamic evolution of the hidden sector, which can be either in thermal equilibrium or out of equilibrium with the bath before the DM freezes out, and moreover, is secluded from the visible sector with small interaction rates generated from the colliders and direct detections. Use of the present mass sets of the hidden sector is motivated by the observed GC gamma-ray excess which can be accounted for by this model via one-step cascade annihilation [17, 19]. More detailed discussions about the GC allowed region, which are constrained by the astrophysical and cosmological measurements as well as the LUX-ZEPLIN projected sensitivity [15], will be presented in Sec. VI.

The rest of this paper is organized as follows. In Sec. II, we start with an introduction of the vector DM model which is UV-complete. In this model, the hidden sector contains an abelian vector dark matter and a complex scalar. The former is a gauge boson associated with a dark (hidden) gauge symmetry  $U_X(1)$ , while the latter is charged under  $U_X(1)$ . In Sec. III, the model parameters constrained by direct detection and collider experiments will be described first. In Sec. IV, we present a general description of Boltzmann equation in the framework of an expanding Universe which is homogeneous and isotropic. We further consider the moments of Boltzmann

equations that are relevant to the evolutions of the number densities and temperatures for the hidden species. In Sec. V, two sets of mass parameters which can account for the GC gamma-ray excess are used in the numerical analyses. The results are given and discussed. The parameter space relevant to the GC gamma-ray excess and concerning the current limits and prospects are further discussed in Sec. VI. In Sec. VII, we draw the conclusions. All technical derivations are collected in Appendices.

## II. THE MODEL

The simplest secluded vector dark matter can be made of the abelian gauge bosons,  $X_\mu$ 's, which get the mass from the vacuum expectation value (VEV) of the hidden complex scalar field  $\Phi_S$  due to the spontaneously dark gauge symmetry  $U_X(1)$  breaking, where the  $Z_2$  symmetry,  $X_\mu \rightarrow -X_\mu$  and  $\Phi_S \rightarrow \Phi_S^*$ , is imposed to stabilize the dark matter [17]. The relevant kinetic Lagrangian ( $\mathcal{L}_{\text{kinetic}}$ ) and the scalar potential ( $\mathcal{L}_{\text{scalar}}$ ) are given by

$$\mathcal{L}_{\text{kinetic}} \supset -\frac{1}{4}X_{\mu\nu}X^{\mu\nu} + (D_\mu\Phi_S)^\dagger(D^\mu\Phi_S), \quad (1)$$

$$\mathcal{L}_{\text{scalar}} = -\mu_H^2|\Phi_H|^2 - \mu_S^2|\Phi_S|^2 - \frac{\lambda_H}{2}(\Phi_H^\dagger\Phi_H)^2 - \frac{\lambda_S}{2}(\Phi_S^\dagger\Phi_S)^2 - \lambda_{HS}(\Phi_H^\dagger\Phi_H)(\Phi_S^\dagger\Phi_S), \quad (2)$$

where  $\Phi_H = (H^+, H^0)^T$  is the SM Higgs doublet,  $X_{\mu\nu} = \partial_\mu X_\nu - \partial_\nu X_\mu$ , and the covariant derivative is defined as  $D_\mu\Phi_S = (\partial_\mu + i\lambda_X Q_{\Phi_S} X_\mu)\Phi_S$ , with  $Q_{\Phi_S}$  the  $U_{\text{dm}}(1)$  charge of  $\Phi_S$ . After spontaneous symmetry breaking, the Higgs fields develop non-zero VEV's,

$$\Phi_H = \frac{1}{\sqrt{2}}(v_H + \phi_h + i\sigma_h), \quad \Phi_S = \frac{1}{\sqrt{2}}(v_S + \phi_s + i\sigma_s), \quad (3)$$

where the CP-odd states,  $\sigma_h$  and  $\sigma_s$ , respectively becomes the longitudinal components of the  $Z$  boson and  $X_\mu$ ; the dark matter thus obtain a mass,  $m_X = \lambda_X Q_{\Phi_S} v_S$ . In the present paper, we will simply use  $Q_{\Phi_S} = 1$ .

The scalar fields  $(\phi_h, \phi_s)$  can be expressed in terms of mass eigenstates of physical Higgses  $(h, S)$  as

$$\begin{pmatrix} \phi_h \\ \phi_s \end{pmatrix} = \begin{pmatrix} \cos\alpha & -\sin\alpha \\ \sin\alpha & \cos\alpha \end{pmatrix} \begin{pmatrix} h \\ S \end{pmatrix}, \quad (4)$$

and the mass squared matrix in the former basis can be parametrized in terms of masses of the latter and the mixing angle  $\alpha$ ,

$$\begin{pmatrix} \lambda_H v_H^2 & \lambda_{HS} v_S v_H \\ \lambda_{HS} v_S v_H & \lambda_S v_S^2 \end{pmatrix} = \begin{pmatrix} m_h^2 c_\alpha^2 + m_S^2 s_\alpha^2 & (m_h^2 - m_S^2) s_\alpha c_\alpha \\ (m_h^2 - m_S^2) s_\alpha c_\alpha & m_S^2 c_\alpha^2 + m_h^2 s_\alpha^2 \end{pmatrix}. \quad (5)$$

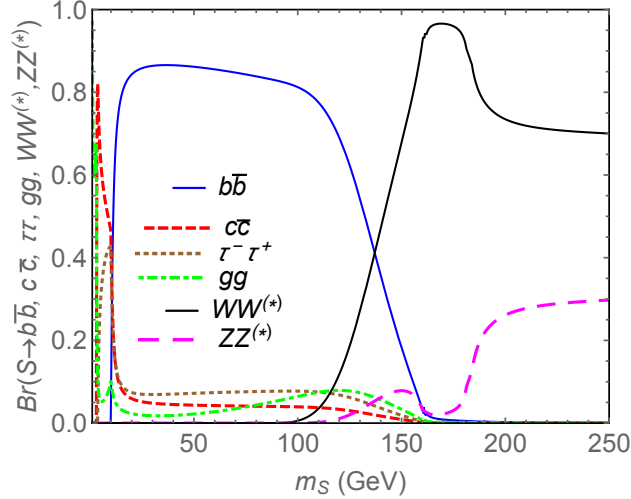


FIG. 1. The main branching ratios of the hidden mediator  $S$  with  $m_S < 250$  GeV.

Here and throughout the paper, we adopt the abbreviations:  $s_\alpha \equiv \sin \alpha$  and  $c_\alpha \equiv \cos \alpha$ . Using  $v_H \simeq 246$  GeV and  $m_h = 125.18$  GeV [35], we will take  $m_X, m_S, \lambda_X$  and  $\alpha$  as the independent parameters in the following analysis.

The branching ratios of the hidden scalar,  $S$ , with a mass of  $m_S \lesssim 2m_h$ , are depicted in Fig. 1, where, in the range giving the good fit to the GC gamma-excess data, the scalar mass satisfies  $m_S \lesssim m_X \lesssim 130$  GeV. The related partial widths of the hidden scalar  $S$  are summarized and discussed in Appendix A, where the results are relevant to the studies of the relic abundance and indirect detection searches.

### III. DIRECT DETECTION AND LHC CONSTRAINTS

In this paper, we will use two sets of the masses for the dark matter and mediator: (i)  $m_X = 80$  GeV,  $m_S = 0.8m_X = 64$  GeV, and (ii)  $m_X = 80$  GeV,  $m_S = 0.99m_X = 79.2$  GeV, to study the thermal evolution of the hidden sector. These two sets can provide a good fit to the GC gamma-ray excess data. For the first set, when the hidden sector with a sizable mass gap undergoes the cannibal process, the down-scattering rate,  $XX \rightarrow SS$ , can be significantly larger than the up-scattering one,  $SS \rightarrow XX$ . For the second set, the hidden sector is nearly degenerate, and can be further constrained by the gamma-line searches at the indirect detection. Moreover, because the low-velocity DM annihilation cross section is zero in  $m_S \rightarrow m_X$  limit, a larger  $X$ - $S$  coupling is needed to account for the GC data and the DM relic abundance.

In the secluded DM model, the direct detection measurements and colliders weakly constrain

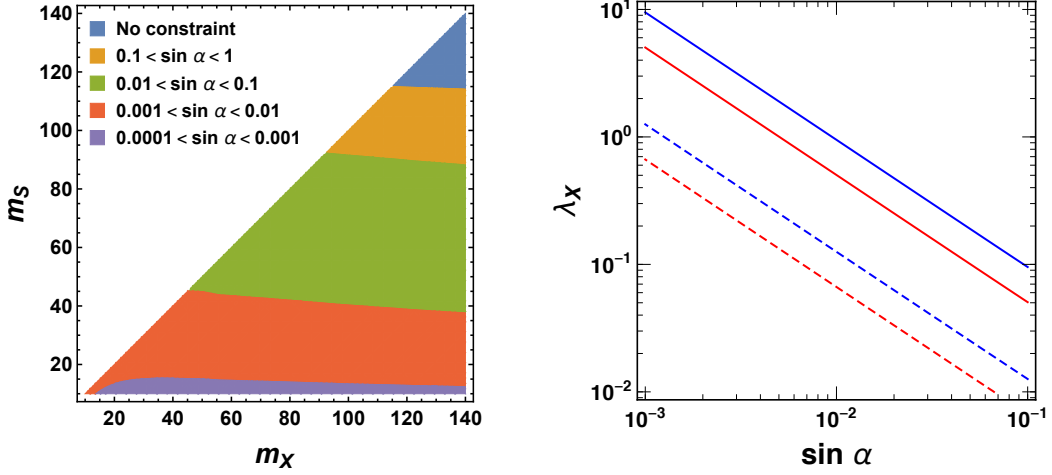


FIG. 2. Left panel: The region with  $m_X > m_S$  on the  $(m_X, m_S)$  plane, where, by using  $\lambda_X = 0.173$ , the XENON1T [12] allowed range of  $\sin \alpha$  is given. Right panel: Bounds of  $\sin \alpha$  and  $\lambda_X$  from XENON1T and LZ projected sensitivity [15] denoted by the solid and dashed lines, respectively, where the red line is for  $m_X = 80$  GeV,  $m_S = 0.8m_X$ , and the blue for  $m_X = 80$  GeV,  $m_S = 0.99m_X$ .

the parameter region allowed by the GC excess result. The spin-independent cross section for a vector dark matter particle scattering off a single nucleon via a scalar mediator  $S$  exchange is given by

$$\sigma_N = \frac{\mu_{XN}^2 m_N^2 f_N^2 \lambda_X^2}{4\pi} \frac{\sin^2 2\alpha}{v_H^2} \left( \frac{1}{m_S^2} - \frac{1}{m_h^2} \right)^2, \quad (6)$$

where  $\mu_{XN}$  is the reduced mass of the dark matter and nucleon,  $f_N = \sum_q \langle N | \bar{q}q | N \rangle m_q / m_N \simeq 0.3$  [36]. The parameter space constrained by XENON1T [12] is shown in Fig. 2, where in the right panel the bound by the LUX-ZEPLIN (LZ) projected sensitivity [15] is shown. The constraint from the invisible Higgs decay, which is less than 25% at the 95% CL [35], is much weaker than that from direct detection. Meanwhile, for the present case,  $h \rightarrow SS$  is kinematically forbidden.

#### IV. THERMAL EVOLUTION OF THE NONRELATIVISTIC HIDDEN PARTICLES

The evolution of the phase space distribution  $f_h$  (with  $h \equiv X$  or  $S$ ) of the hidden sector particles in the homogeneous isotropic Friedmann-Robertson-Walker Universe is described by the Boltzmann equation,

$$\frac{\partial f_h}{\partial t} - H p \frac{\partial f_h}{\partial p} = C[f_h], \quad (7)$$

where  $H$  is the Hubble expansion parameter,  $p = \sqrt{E_h^2 - m_h^2}$  is the momentum of the hidden particle, and  $C[f_h]$  is the collision term. During the process of the thermal evolution, the distribution of the hidden sector particles follows Bose-Einstein statistics,

$$f_h(E_h, T_h) = \frac{1}{e^{(E_h - \mu_h)/T_h} - 1}, \quad (8)$$

with  $\mu_h$  the chemical potential of the particle species  $h$ . In the present case, we consider  $m_X \gtrsim m_S \sim \mathcal{O}(10 - 100 \text{ GeV})$  and the thermal evolution that the elastic scattering  $\chi S \leftrightarrow \chi S$  can keep the  $X$  and  $S$  particles in thermal equilibrium ( $T_X = T_S$ ) until kinetic decoupling temperature  $T_X^{\text{kd}} \equiv T_X(a_X^{\text{kd}})$ , below that we have  $T_X(a) \simeq T_X^{\text{kd}} \cdot (a_X^{\text{kd}}/a)^2$ , where  $a$  is the cosmic scale factor and  $a_X^{\text{kd}}$  is its corresponding value at  $T_X^{\text{kd}}$ .

For a hidden sector particle,  $h_1$ , the generic form of one of the collision terms described by the interaction “ $h_1 h_2 \cdots b_1 b_2 \cdots \leftrightarrow h'_1 h'_2 \cdots b'_1 b'_2 \cdots$ ” can be written as

$$\begin{aligned} C[f_{h_1}] = & \frac{1}{2E_{h_1} g_{h_1}} \int d\Pi_{h_2} \cdots d\Pi_{b_1} d\Pi_{b_2} \cdots d\Pi_{h'_1} d\Pi_{h'_2} \cdots d\Pi_{b'_1} d\Pi_{b'_2} \cdots \\ & \times (2\pi)^4 \delta^{(4)}(p_{h_1} + p_{h_2} + \cdots + p_{b_1} + p_{b_2} + \cdots - p_{h'_1} - p_{h'_2} - \cdots - p_{b'_1} - p_{b'_2} - \cdots) |M|^2 \\ & \times \frac{\Delta - \Delta'}{S_y S'_y} \left[ f_{h'_1} f_{h'_2} \cdots f_{b'_1} f_{b'_2} \cdots (1 + f_{h_1})(1 + f_{h_2}) \cdots (1 \pm f_{b_1})(1 \pm f_{b_2}) \right. \\ & \left. - f_{h_1} f_{h_2} \cdots f_{b_1} f_{b_2} \cdots (1 + f_{h'_1})(1 + f_{h'_2}) \cdots (1 \pm f_{b'_1})(1 \pm f_{b'_2}) \right], \end{aligned} \quad (9)$$

where

$$d\Pi_i \equiv \frac{d^3 p_i}{(2\pi)^3 2E_i}, \quad (10)$$

$h_i^{(\prime)}$  is the particle of the hidden sector with temperature  $T_X$  for  $X$  or  $T_S$  for  $S$ ,  $b_i^{(\prime)}$  is the relativistic SM particle with temperature  $T$ ,  $|M|^2$  invariant under times reversal and reflection is the square of the amplitude summed over the internal degrees of freedom (dof),  $g_i$ , of all the initial and final particles,  $S_y$  and  $S'_y$  are the symmetric factors in the initial and final states, respectively,  $\Delta$  and  $\Delta'$  are the numbers of the species which are the same as  $h_1$  and participate in the interaction in the initial and final states, respectively; note that if the particle composition in the initial state is exactly the same as that in the final state (*e.g.* elastic scattering  $S + \text{SM} \leftrightarrow S + \text{SM}$ , and elastic self-scattering  $SS \leftrightarrow SS$ ), the moment result can be non-vanishing (see Eq. (31) for instance), and an additional factor “1/2” needs to be added in  $C[f_{h_1}]$  to avoid double-counting. Taking  $SSS \leftrightarrow XX$  as an example, we have  $S_y \equiv 3!$ , and  $S'_y \equiv 2!$ . Moreover, we have  $\Delta \equiv 3, \Delta' \equiv 0$  for considering the Boltzmann equation of the  $S$  particles, while  $\Delta \equiv 0, \Delta' \equiv 2$  for  $X$ . Here the

$1 \pm f_i$  terms with plus and minus signs encode the influence due to Bose enhancement and Pauli blocking, respectively.

We are interested in reactions dominated by the phase space region where the average number of particles in a single-particle state is much less than 1, i.e.,  $1 \pm f_i \simeq 1$ , and thus approximate the distributions as

$$f_i = e^{-(E_i - \mu_i)/T_i} (1 \pm f_i) \simeq e^{-(E_i - \mu_i)/T_i}. \quad (11)$$

Basically, this is a good approximation even for high or low temperature. The collision term can be then given as the following form,

$$\begin{aligned} C[f_{h_1}] = & \frac{1}{2E_{h_1}g_{h_1}} \int d\Pi_{h_2} \dots d\Pi_{b_1} d\Pi_{b_2} \dots d\Pi_{h'_1} d\Pi_{h'_2} \dots d\Pi_{b'_1} d\Pi_{b'_2} \dots \\ & \times (2\pi)^4 \delta^{(4)}(p_{h_1} + p_{h_2} + \dots + p_{b_1} + p_{b_2} + \dots - p_{h'_1} - p_{h'_2} - \dots - p_{b'_1} - p_{b'_2} - \dots) |M|^2 \\ & \times \frac{\Delta - \Delta'}{S_y S'_y} \left[ f_{h'_1}(T_{h_1}) f_{h'_2}(T_{h_2}) \dots f_{b'_1}(T) f_{b'_2}(T) \dots - f_{h_1}(T_{h_1}) f_{h_2}(T_{h_2}) \dots f_{b_1}(T) f_{b_2}(T) \dots \right], \quad (12) \end{aligned}$$

where  $f_i(T_i) \equiv f_i(E_i, T_i)$ . It should be noted that the relativistic SM,  $X$  and  $S$  are defined by the different temperatures,  $T, T_X$  and  $T_S$ , respectively. In our case, the dark matter and mediator are in thermal equilibrium, i.e.  $T_X = T_S$ , until their kinetic decoupling; we will further discuss this point in the following sections.

#### A. The Boltzmann moment equation for the number densities of hidden sector particles

To get the coupled Boltzmann equations for the number densities of  $X$  and  $S$ , we form the moment by multiplying Eq. (7) with “1” and integrating over the momentum space,

$$n_X(T_X) = g_X \int \frac{d^3 p_X}{(2\pi)^3} f_X(T_X), \quad n_S(T_S) = g_S \int \frac{d^3 p_S}{(2\pi)^3} f_S(T_S). \quad (13)$$

In our case, the sufficiently large interactions within the hidden sector can maintain thermal equilibrium among the hidden sector particles, i.e.,  $T_X = T_S$ , before the DM freezes out. The resulting equations of number densities are given by

$$\begin{aligned} \frac{dn_X}{dt} + 3Hn_X = & -\langle \sigma v \rangle_{XX \rightarrow SS} \left( n_X^2 - (n_X^{\text{eq}})^2 \frac{n_S^2}{(n_S^{\text{eq}})^2} \right) - \frac{1}{3} \langle \sigma v^2 \rangle_{XXX \rightarrow XS} \left( n_X^3 - n_X n_S \frac{(n_X^{\text{eq}})^2}{n_S^{\text{eq}}} \right) \\ & - \langle \sigma v^2 \rangle_{XXS \rightarrow SS} \left( n_X^2 n_S - (n_X^{\text{eq}})^2 \frac{n_S^2}{(n_S^{\text{eq}})^2} \right) + \frac{1}{3} \langle \sigma v^2 \rangle_{SSS \rightarrow XX} \left( n_S^3 - (n_S^{\text{eq}})^3 \frac{n_X^2}{(n_X^{\text{eq}})^2} \right), \quad (14) \end{aligned}$$



$$\begin{aligned}
\frac{dn_S}{dt} + 3Hn_S = & -\Gamma_S \left( \frac{K_1(x_S \cdot m_S/m_X)}{K_2(x_S \cdot m_S/m_X)} n_S - \frac{K_1(x \cdot m_S/m_X)}{K_2(x \cdot m_S/m_X)} n_S^{\text{eq}}(T) \right) \\
& - \left( \langle \sigma v \rangle_{SS \rightarrow \sum_{ij} \text{SM}_i \text{SM}_j} n_S^2 - \langle \sigma v \rangle_{SS \rightarrow \sum_{ij} \text{SM}_i \text{SM}_j}(T) (n_S^{\text{eq}}(T))^2 \right) \\
& + \langle \sigma v \rangle_{XX \rightarrow SS} \left( n_X^2 - (n_X^{\text{eq}})^2 \frac{n_S^2}{(n_S^{\text{eq}})^2} \right) + \frac{1}{6} \langle \sigma v^2 \rangle_{XXX \rightarrow XS} \left( n_X^3 - n_X n_S \frac{(n_X^{\text{eq}})^2}{n_S^{\text{eq}}} \right) \\
& + \frac{1}{2} \langle \sigma v^2 \rangle_{XXS \rightarrow SS} \left( n_X^2 n_S - (n_X^{\text{eq}})^2 \frac{n_S^2}{(n_S^{\text{eq}})^2} \right) - \frac{1}{2} \langle \sigma v^2 \rangle_{XSS \rightarrow XS} \left( n_X n_S^2 - n_X n_S n_S^{\text{eq}} \right) \\
& - \frac{1}{2} \langle \sigma v^2 \rangle_{SSS \rightarrow XX} \left( n_S^3 - (n_S^{\text{eq}})^3 \frac{n_X^2}{(n_X^{\text{eq}})^2} \right) - \frac{1}{6} \langle \sigma v^2 \rangle_{SSS \rightarrow SS} \left( n_S^3 - n_S^2 n_S^{\text{eq}} \right), \quad (15)
\end{aligned}$$

where  $K_i$  is the modified Bessel function of the second kind with  $x_S \equiv m_X/T_S$  and  $x \equiv m_X/T$ ,  $n_i^{\text{eq}}$  is the equilibrium number density with vanishing chemical potential,  $\Gamma_S$  is the total decay width of  $S$  into SM final states, and  $\langle \sigma v \rangle_i$  and  $\langle \sigma v^2 \rangle_i$  are respectively the thermally averaged cross sections for  $2 \rightarrow 2$  and  $3 \rightarrow 2$  annihilation processes denoted by the subscript “ $i$ ”; the details for these results are given in Appendices B and C. Note that only the terms involving  $n_S^{\text{eq}}$  and, meanwhile, relevant to  $S \rightarrow \text{SM}_i \text{SM}_i$  and  $SS \rightarrow \text{SM}_i \text{SM}_i$  on the right-hand side (RHS) of Eq. (15) are functions of the bath temperature, “ $T$ ”, which is explicitly indicated, whereas the remaining ones appearing in Eqs. (14) and (15) are functions of “ $T_S$ ” or “ $T_X$ ”. Here and in the following analysis, we will use  $T_X = T_S$  due to the fact that the hidden sector particles keep thermal equilibrium before the DM freeze-out.

Because the comoving number density of dark matter is conserved after freeze-out, we introduce the normalized yields for the hidden sector,

$$y_X(x_X; x) = \sqrt{\frac{\pi}{45G}} m_X g_*^{1/2}(m_X) \langle \sigma v \rangle_{XX \rightarrow SS}^{(0)} Y_X(x_X; x), \quad (16)$$

$$y_S(x_S; x) = \sqrt{\frac{\pi}{45G}} m_X g_*^{1/2}(m_X) \langle \sigma v \rangle_{XX \rightarrow SS}^{(0)} Y_S(x_S; x), \quad (17)$$

with  $x_i \equiv m_X/T_i$  and  $x \equiv m_X/T$  being the temperature variables of the hidden sector particles and thermal bath, respectively, the yields  $Y_i \equiv n_i(T_i)/s(T)$  being the number density normalized by the total entropy density, and  $g_*$  being the effectively total number of relativistic dof; see below for definition. Here  $\langle \sigma v \rangle_{XX \rightarrow SS}^{(0)}$  is the leading approximation of  $\langle \sigma v \rangle_{XX \rightarrow SS}$  which is s-wave. In the following discussion, we will simply use  $y_i(x_i) \equiv y_i(x_i; x)$ . We use  $x \equiv m_X/T$  as the evolution variable and trade the time derivative in the Boltzmann equations to be

$$\frac{d}{dt} = \frac{m_X^2}{x} \left( \frac{8\pi^3 G}{90} \right)^{1/2} \frac{h_{\text{eff}}}{g_*^{1/2}} \frac{d}{dx}, \quad (18)$$

where the relativistic degrees of freedom,  $h_{\text{eff}}$  and  $g_*^{1/2} \equiv \tilde{h}_{\text{eff}}/g_{\text{eff}}^{1/2}$  with

$$\tilde{h}_{\text{eff}} \equiv h_{\text{eff}} [1 + (1/3)(d \ln h_{\text{eff}}/d \ln T)], \quad (19)$$

are defined via

$$s(T) = \frac{2\pi^2}{45} h_{\text{eff}}(T) T^3, \quad \rho(T) = \frac{\pi^2}{30} g_{\text{eff}}(T) T^4. \quad (20)$$

Thus, we can further rewrite the Boltzmann equations to be

$$\begin{aligned} \frac{dy_X}{dx} = & -\frac{\delta_{\text{XS}} \delta_{\text{dof}}}{x^2} \left( y_X^2 - (y_X^{\text{eq}})^2 \frac{y_S^2}{(y_S^{\text{eq}})^2} \right) \\ & + \frac{\delta_{\text{dof}}}{x^5} \frac{\pi}{\sqrt{90}} \frac{h_{\text{eff}}(T)}{g_*^{1/2}(m_X)} \frac{m_X^2}{M_{\text{pl}}} \left[ -\frac{1}{3} \frac{\langle \sigma v^2 \rangle_{XX \rightarrow XS}}{(\langle \sigma v \rangle_{XX \rightarrow SS}^{(0)})^2} \left( y_X^3 - y_X (y_X^{\text{eq}})^2 \frac{y_S}{y_S^{\text{eq}}} \right) \right. \\ & \left. + \frac{1}{3} \frac{\langle \sigma v^2 \rangle_{SS \rightarrow XX}}{(\langle \sigma v \rangle_{XX \rightarrow SS}^{(0)})^2} \left( y_S^3 - \frac{y_X^2}{(y_X^{\text{eq}})^2} (y_S^{\text{eq}})^3 \right) - \frac{\langle \sigma v^2 \rangle_{XS \rightarrow SS}}{(\langle \sigma v \rangle_{XX \rightarrow SS}^{(0)})^2} \left( y_X^2 y_S - \frac{y_S^2}{y_S^{\text{eq}}} (y_X^{\text{eq}})^2 \right) \right], \quad (21) \end{aligned}$$

$$\begin{aligned} \frac{dy_S}{dx} = & -x \frac{\sqrt{90}}{\pi} M_{\text{pl}} \frac{g_*^{1/2}(T)}{h_{\text{eff}}(T)} \frac{\Gamma_S}{m_X^2} \left( \frac{K_1(x_S \cdot m_S/m_X)}{K_2(x_S \cdot m_S/m_X)} y_S - \frac{K_1(x \cdot m_S/m_X)}{K_2(x \cdot m_S/m_X)} y_S^{\text{eq}}(x) \right) \\ & - \frac{\delta_{\text{dof}}}{x^2 \langle \sigma v \rangle_{XX \rightarrow SS}^{(0)}} \left[ \langle \sigma v \rangle_{SS \rightarrow \sum_i \text{SM}_i \text{SM}_i} y_S^2 - \langle \sigma v \rangle_{SS \rightarrow \sum_i \text{SM}_i \text{SM}_i}(x) (y_S^{\text{eq}}(x))^2 \right] \\ & - \frac{\delta_{\text{XS}} \delta_{\text{dof}}}{x^2} \left[ \frac{(y_X^{\text{eq}})^2}{(y_S^{\text{eq}})^2} y_S^2 - y_X^2 \right] + \frac{\delta_{\text{dof}}}{x^5} \frac{\pi}{\sqrt{90}} \frac{h_{\text{eff}}(T)}{g_*^{1/2}(m_X)} \frac{m_X^2}{M_{\text{pl}}} \left[ \frac{1}{6} \frac{\langle \sigma v^2 \rangle_{XX \rightarrow XS}}{(\langle \sigma v \rangle_{XX \rightarrow SS}^{(0)})^2} \left( y_X^3 - y_X (y_X^{\text{eq}})^2 \frac{y_S}{y_S^{\text{eq}}} \right) \right. \\ & + \frac{1}{2} \frac{\langle \sigma v^2 \rangle_{XS \rightarrow SS}}{(\langle \sigma v \rangle_{XX \rightarrow SS}^{(0)})^2} \left( y_X^2 y_S - \frac{y_S^2}{y_S^{\text{eq}}} (y_X^{\text{eq}})^2 \right) - \frac{1}{2} \frac{\langle \sigma v^2 \rangle_{XS \rightarrow XS}}{(\langle \sigma v \rangle_{XX \rightarrow SS}^{(0)})^2} \left( y_X y_S^2 - y_X y_S y_S^{\text{eq}} \right) \\ & \left. - \frac{1}{2} \frac{\langle \sigma v^2 \rangle_{SS \rightarrow XX}}{(\langle \sigma v \rangle_{XX \rightarrow SS}^{(0)})^2} \left( y_S^3 - \frac{y_X^2}{(y_X^{\text{eq}})^2} (y_S^{\text{eq}})^3 \right) - \frac{1}{6} \frac{\langle \sigma v^2 \rangle_{SS \rightarrow SS}}{(\langle \sigma v \rangle_{XX \rightarrow SS}^{(0)})^2} \left( y_S^3 - y_S^2 y_S^{\text{eq}} \right) \right], \quad (22) \end{aligned}$$

where  $M_{\text{pl}} \equiv (8\pi G)^{-1/2} = 2.44 \times 10^{18}$  GeV is the reduced Planck mass,

$$\delta_{\text{XS}} \equiv \frac{\langle \sigma v \rangle_{XX \rightarrow SS}(T_X)}{\langle \sigma v \rangle_{XX \rightarrow SS}^{(0)}}, \quad \delta_{\text{dof}} \equiv \frac{g_*^{1/2}(T)}{g_*^{1/2}(m_X)}, \quad (23)$$

and the equilibrium value of  $y_i$  is given by

$$y_i^{\text{eq}}(x_i) \equiv y_i^{\text{eq}}(x_i; x) = g_i \frac{\sqrt{90}}{2\pi^3} M_{\text{pl}} \frac{g_*^{1/2}(m_X)}{h_{\text{eff}}(T)} m_X \left( x \frac{m_i}{m_X} \right)^2 \frac{x}{x_i} \langle \sigma v \rangle_{XX \rightarrow SS}^{(0)} K_2 \left( x_i \frac{m_i}{m_X} \right). \quad (24)$$

Again, it should be noted that in Eq. (22) the terms involving  $y_S^{\text{eq}}$ 's and relevant to  $S \rightarrow \text{SM}_i \text{SM}_i$  and  $SS \rightarrow \text{SM}_i \text{SM}_i$  are functions only of “ $x$ ”, as shown explicitly, while other quantities appearing Eqs. (21) and (22) are instead defined as functions of “ $x_S$ ”, which are not shown explicitly, before freeze-out. In the following section, we will exhibit the evolution of  $T_S/T$  as a function of  $x$ , i.e., a function of the bath temperature  $T$ .

The relic abundance is found to be

$$\Omega_{\text{DM}} = \frac{Y_X^\infty s_0 m_X}{\rho_c} \simeq \frac{1.04 \times 10^9 \text{ GeV}^{-1}}{\sqrt{8\pi g_*(m_X)} M_{\text{pl}} h^2} \frac{y_X^\infty}{\langle \sigma v \rangle_{XX \rightarrow SS}^{(0)}}, \quad (25)$$

which can be determined by matching the present-day DM relic abundance  $\Omega_{\text{DM}} = (0.1198 \pm 0.0026)/h^2$  [35, 37], where  $Y_X^\infty$  is related to  $y_X^\infty = y_X(x \rightarrow \infty)$  (see also Eq. (16)),  $s_0 = 2891 \text{ cm}^{-3}$  is the visible entropy density today,  $\rho_c = 3H_0^2/(8\pi G)$  is the critical energy density, and  $h \simeq 0.678$  is the Hubble constant  $H_0$  of the present day in units of  $100 \text{ km s}^{-1} \text{ Mpc}^{-1}$ .  $y_X^\infty$  is related to  $x = x_f (\equiv m_X/T_f)$  with  $T_f$  the freeze-out temperature, and can be understood as follows. Well after DM freeze-out, which occurs at  $x = x_f$ , the Boltzmann equation in Eq. (21) can be approximated as

$$\frac{dy_X}{dx} \approx - \frac{\delta_{XS}\delta_{\text{dof}}}{x^2} y_X^2. \quad (26)$$

Solving the equation, we get

$$y_X^\infty = \left( \int_{x_f}^{\infty} \frac{\delta_{XS}\delta_{\text{dof}}}{x^2} dx \right)^{-1} = g_*^{1/2}(m_X) \langle \sigma v \rangle_{XX \rightarrow SS}^{(0)} \left( \int_{x_f}^{\infty} \frac{g_*^{1/2}(T) \langle \sigma v \rangle_{XX \rightarrow SS}(T_X)}{x^2} dx \right)^{-1}, \quad (27)$$

where we use the fact that the value of  $y_X$  at  $x = x_f$  is significantly larger than  $y_X^\infty$ , and we can approximate  $T_X \approx T_S$  in the calculation (see Figs. 3 and 4 for the temperature dependence in the next section).

### B. The Boltzmann moment equation for $T_S/T$

We consider the case that the DM can be kept in thermal equilibrium with the hidden scalar before DM freeze out, but may be highly decoupled from the SM thermal bath. Here we focus on the study about the temperature evolution of the hidden scalar  $S$ , and then discuss the DM temperature evolution after freeze out. The temperature evolution of nonrelativistic  $S$  is relevant to the following elastic scattering and (species) number changing interactions — (i) annihilation:  $SS \leftrightarrow \text{SM SM}$ , (ii) elastic scattering:  $S + \text{SM} \leftrightarrow S + \text{SM}$ , (iii) cannibalization including  $SSS \leftrightarrow SS$ ,  $XSS \leftrightarrow XS$ ,  $XXS \leftrightarrow SS$ ,  $SSS \leftrightarrow XX$ , and  $XXX \leftrightarrow XS$ , and (iv) decay:  $S \leftrightarrow \text{SM SM}$ .

We adopt the definition of the temperature,

$$T_S = \frac{g_S}{n_S(T_S)} \int \frac{d^3p}{(2\pi)^3} \frac{\mathbf{p}_S^2}{3E_S} f_S(T_S), \quad (28)$$

which is suitable not only for the nonrelativistic case at low temperatures,  $T < m_S$ , but also for relativistic case at high temperature,  $T \lesssim m_S/0.01$ . The Boltzmann moment equation of the hidden scalar's temperature can be formed by multiplying Eq. (7) with  $\mathbf{p}^2/(3E_S)$  and then integrating over the momentum space. Thus, we arrive at the form of the temperature evolution equation,

$$\frac{dT_S}{dt} + (2 - \delta_H) H T_S = \frac{1}{n_S(T_S)} \left[ - \left( \frac{dn_S(T_S)}{dt} + 3H n_S(T_S) \right) T_S + g_S \int d\Pi_S C \left[ f_S \cdot \frac{\mathbf{p}_S^2}{3E_S} \right] \right], \quad (29)$$

where

$$\delta_H(T_S) \equiv 1 - \frac{1}{n_S(T_S) T_S} \int \frac{d^3 p}{(2\pi)^3} \frac{\mathbf{p}_S^2 m_S^2}{3E_S^3} f_S(T_S), \quad (30)$$

which is approximately to be “0” for nonrelativistic particles or “1” for ultra-relativistic ones. Here we have denoted the collision term as  $C[f_S \cdot E_S]$  which is related to  $C[f_S]$  (see Eq. (9) or (12)) with the replacement

$$\Delta - \Delta' \rightarrow \Delta \cdot \frac{\mathbf{p}_S^2}{3E_S} - \Delta' \cdot \frac{\mathbf{p}_S'^2}{3E_S'}, \quad (31)$$

corresponding to a process  $i(\text{initial state}) \leftrightarrow f(\text{final state})$  with a prime for the final state. In the following, the collision term due to various interactions will be discussed term by term in details.

After the hidden sector is chemically decoupled from the bath, i.e., its number density production rate is less the expanding rate of the Universe, we have  $n_h a^3 = \text{constant}$  from Eqs. (14) and (15) if cannibalization can be neglected. Moreover, well after the cannibal epoch, if the nonrelativistic hidden sector is out of thermal equilibrium with the bath, we have  $T_h a^2 = \text{constant}$  as read from Eq. (29).

### 1. The collision term due to $SS \leftrightarrow SM_1 SM_2$

The collision term resulting from  $S(p_{S,1})S(p_{S,2}) \leftrightarrow SM_1(p_{1'}) SM_2(p_{2'})$  is given by

$$\begin{aligned} g_S \int \frac{d^3 p_S}{(2\pi)^3} C \left[ f_S \cdot \frac{\mathbf{p}_S^2}{3E_S} \right]_{SS \leftrightarrow SM_1 SM_2} &= \int \prod_i d\Pi_{S,i} d\Pi_{i'} (2\pi)^4 \delta^{(4)}(p_{S,1} + p_{S,2} - p_{1'} - p_{2'}) \\ &\times \frac{2}{2!m!} \frac{\mathbf{p}_{S,1}^2}{3E_{S,1}} \left[ e^{-(E_{1'}+E_{2'})/T} - e^{2\mu_S/T_S} e^{-(E_{S,1}+E_{S,2})/T_S} \right] |M|_{SS \rightarrow SM_1 SM_2}^2 \\ &\simeq - \left[ T_S \langle \sigma v \rangle_{SS \rightarrow SM_1 SM_2}(T_S) (n_S(T_S))^2 - T \langle \sigma v \rangle_{SS \rightarrow SM_1 SM_2}(T) (n_S^{\text{eq}}(T))^2 \right], \end{aligned} \quad (32)$$

where  $m! = 2$  for identical final state particles or 1 otherwise. Here we have used the energy conservation  $E_{1'} + E_{2'} = E_{S,1} + E_{S,2}$ , and the relation,

$$e^{\mu_S/T(S)} = \frac{n_S(T(S))}{n_S^{\text{eq}}(T(S))}. \quad (33)$$

### 2. The collision term due to $S \leftrightarrow SM_1 SM_2$

The collision term resulting from  $S(p_S) \leftrightarrow SM_1(p_{1'}) SM_2(p_{2'})$  is given by

$$\begin{aligned}
g_S \int \frac{d^3 p_S}{(2\pi)^3} C \left[ f_S \cdot \frac{\mathbf{p}_S^2}{3E_S} \right]_{S \leftrightarrow SM_1 SM_2} &= \int d\Pi_S \prod_i d\Pi_{i'} (2\pi)^4 \delta^{(4)}(p_S - p_{1'} - p_{2'}) |M|_{S \rightarrow SM_1 SM_2}^2 \\
&\times \frac{1}{m!} \frac{\mathbf{p}_S^2}{3E_S} \left[ e^{-(E_1+E_2)/T} - e^{\mu_S/T_S} e^{-E_S/T_S} \right] \\
&\simeq -\Gamma_{S \rightarrow SM_1 SM_2} \left[ T_S \frac{c(T_S)}{n_S^{\text{eq}}(T_S)} n_S(T_S) - T \frac{c(T)}{n_S^{\text{eq}}(T)} n_S^{\text{eq}}(T) \right], \tag{34}
\end{aligned}$$

where  $m! = 2$  for identical final state particles or 1 otherwise,  $\Gamma_{S \rightarrow SM_1 SM_2}$  is  $S \rightarrow SM_1 SM_2$  decay width, and

$$c(T) = g_S \frac{m_S}{3T} \int \frac{d^3 p_S}{(2\pi)^3} \frac{\mathbf{p}_S^2}{E_S^2} e^{-E_S/T} = m_S T^2 \frac{g_S}{6\pi^2} \int_{m_S/T}^{\infty} dy \frac{(y^2 - m_S^2/T^2)^{3/2}}{y} e^{-y}, \tag{35}$$

which approaches to  $n_S^{\text{eq}}(T)$  in a nonrelativistic limit. The result of Eq. (34) is also correct if replacing  $\Gamma_{S \rightarrow SM_1 SM_2}$  with the relevant three- (or more-) body decay mode.

### 3. The collision term due to cannibal annihilations among the hidden sector particles

The collision term arising from cannibal annihilations among the hidden sector particles contains the following processes:  $SSS \leftrightarrow SS$ ,  $XSS \leftrightarrow XS$ ,  $XXS \leftrightarrow SS$ ,  $SSS \leftrightarrow XX$ , and  $XXX \leftrightarrow XS$ . Here, the result for  $XSS \leftrightarrow XS$  will be shown, while for the others can be derived in a similar way. When the temperature of the hidden sector drops below  $m_{X,S}$ , the role of the cannibalization becomes important. If the hidden sector kinetically decouples from the bath at  $T \lesssim m_{X,S}$ , its temperature will decrease logarithmically with the cosmic scale factor during cannibalization (see Eq. (60) for discussion). The collision term resulting from  $X(p_X)S(p_{S,1})S(p_{S,2}) \leftrightarrow X(p_{X'})S(p_{S'})$  is given by

$$\begin{aligned}
g_S \int \frac{d^3 p_S}{(2\pi)^3} C \left[ f_S \cdot \frac{\mathbf{p}_S^2}{3E_S} \right]_{XSS \leftrightarrow XS} &= \int d\Pi_X d\Pi_{S,1} d\Pi_{S,2} d\Pi_{X'} d\Pi_{S'} \\
&\times (2\pi)^4 \delta^{(4)}(p_X + p_{S,1} + p_{S,2} - p_{X'} - p_{S'}) |M|_{XSS \rightarrow XS}^2 \\
&\times \frac{1}{2!} \left( \frac{2\mathbf{p}_{S,1}^2}{3E_{S,1}} - \frac{\mathbf{p}_{S'}^2}{3E_{S'}} \right) \left( e^{(\mu_X + \mu_S)/T_S} e^{-(E_{X'} + E_{S'})/T_S} - e^{(\mu_X + 2\mu_S)/T_S} e^{-(E_X + E_{S,1} + E_{S,2})/T_S} \right) \\
&\simeq \frac{m_S(2m_X + m_S)(2m_X + 3m_S)}{4(m_X + 2m_S)(4m_X + 5m_S)} \langle \sigma v^2 \rangle_{XSS \rightarrow XS} \left[ n_X(T_S) (n_S(T_S))^2 - n_X(T_S) n_S(T_h) n_S^{\text{eq}}(T_S) \right], \tag{36}
\end{aligned}$$

where we have used  $p_{S^{(\nu)},i}^\mu = (E_{S^{(\nu)},i}, \mathbf{p}_{S^{(\nu)},i})$  for the  $S$  and  $p_{X^{(\nu)}}^\mu = (E_{X^{(\nu)}}, \mathbf{p}_{X^{(\nu)}})$  for the  $X$ , and have approximated three initial hidden particles ( $XSS$ ) that annihilate or are produced in the

nonrelativistic limit, i.e.,  $E_{S,i} \approx m_S, E_X \approx m_X$ , such that

$$\frac{\mathbf{p}_{S,1}^2}{E_{S,1}} \approx 0, \quad \frac{\mathbf{p}_{S'}^2}{3E_{S'}} \approx \frac{m_S(2m_X + m_S)(2m_X + 3m_S)}{2(m_X + 2m_S)(4m_X + 5m_S)}. \quad (37)$$

#### 4. The collision term due to elastic scattering: $S + SM \leftrightarrow S + SM$

Here we consider the elastic scattering,  $S(p_S) + SM(k) \leftrightarrow S(p_{S'}) + SM(k')$ , where  $p_{S^{(\prime)}}^\mu = (E_{S^{(\prime)}}, \mathbf{p}_{S^{(\prime)}})$ ,  $k^{(\prime)\mu} = (\omega^{(\prime)}, \mathbf{k}^{(\prime)})$  and “SM” stands for one of the relativistic SM particles that can participate the interaction. The collision term for this elastic scattering takes the following form,

$$\begin{aligned} g_S \int \frac{d^3 p_S}{(2\pi)^3} C \left[ f_S \cdot \frac{\mathbf{p}_S^2}{3E_S} \right]_{S SM \leftrightarrow S SM} &= \sum_{SM} \int \frac{d^3 p_S}{(2\pi)^3 2E_S} \frac{d^3 k}{(2\pi)^3 2\omega} \frac{d^3 p_{S'}}{(2\pi)^3 2E_{S'}} \frac{d^3 k'}{(2\pi)^3 2\omega'} \\ &\times (2\pi)^4 \delta^{(4)}(p_S + k - p_{S'} - k') |M|_{S SM \leftrightarrow S SM}^2 \\ &\times \frac{1}{2} \left( \frac{\mathbf{p}_S^2}{3E_S} - \frac{\mathbf{p}_{S'}^2}{3E_{S'}} \right) \left( f_{S'}(T_S) f_{SM'}(T)(1 - f_{SM}(T)) - f_S(T_S) f_{SM}(T)(1 - f_{SM'}(T)) \right), \end{aligned} \quad (38)$$

where the hidden scalar scattering with all relativistic SM fermions is taken into account. Under the typical condition  $m_S \gg T \sim \omega$ , this term can further reduce to a semi-relativistic Fokker-Planck-type equation [38–43],

$$\begin{aligned} g_S \int \frac{d^3 p_S}{(2\pi)^3} C \left[ f_S \cdot \frac{\mathbf{p}_S^2}{3E_S} \right]_{S SM \leftrightarrow S SM} &\simeq \gamma(T) \int \frac{d^3 p_S}{(2\pi)^3} \frac{\mathbf{p}_S^2}{3E_S} \frac{\partial}{\partial \mathbf{p}_S} \cdot \left( \mathbf{p}_S f_S(T_S) + E_S T \frac{\partial f_S(T_S)}{\partial \mathbf{p}_S} \right) \\ &\simeq -(2 - \delta_H(T_S)) \gamma n_S(T_S) (T_S - T), \end{aligned} \quad (39)$$

where the momentum relaxation rate is given by

$$\gamma(T) = \sum_f \frac{1}{6m_S T} \int \frac{d^3 k}{(2\pi)^3} f_f(T)(1 - f_f(T)) \frac{|\mathbf{k}|}{\sqrt{\mathbf{k}^2 + m_f^2}} \int_{-4\mathbf{k}^2}^0 dt (-t) \frac{d\sigma_{Sf \rightarrow Sf}}{dt}, \quad (40)$$

for which the sum runs over all relevant relativistic SM species, and the differential elastic scattering cross section is

$$\frac{d\sigma_{Sf \rightarrow Sf}}{dt} = \frac{1}{64\pi m_S^2 \mathbf{k}^2} |M_{Sf \rightarrow Sf}|^2, \quad (41)$$

with  $|M_{Sf \rightarrow Sf}|^2$  the square of the scattering amplitude summed over initial and final spine states. Note that in Eq. (40), we have followed the approach given in Ref. [40] to adopt the  $t$ -average matrix  $(8\mathbf{k}^4)^{-1} \int_{-4\mathbf{k}^2}^0 dt (-t) d\sigma/dt$  due to that the scattering amplitude squared in our case vanishes around  $t = 0$  in the relativistic limit  $m_f \rightarrow 0$ ; therefore, it is unsuitable to take the result at zero momentum transfer of the  $t$ -channel as done in Ref. [38].

Taking into account the elastic scattering  $Sf \rightarrow Sf$  which is dominated by the amplitudes with the SM Higgs or hidden scalar mediated in the  $t$ -channel, we find the amplitude squared to be

$$|M_{Sf \rightarrow Sf}|^2 = N_c^f (4m_f^2 - t) \left( \frac{g_{SSS} g_{Sff}}{t - m_S^2} + \frac{g_{hSS} g_{hff}}{t - m_h^2} \right)^2, \quad (42)$$

with  $N_c^f \equiv 3$  (1) for quarks (leptons), and the couplings shown in Eqs. (B2), (B5), (B6), and (B7). Averaging over  $t$  for the scattering amplitude squared, we get the momentum relaxation rate to be

$$\gamma(T) \simeq \sum_f \frac{80 N_c^f m_S}{\pi^3} \left( \frac{g_{SSS} g_{Sff}}{m_S} + \frac{m_S}{m_h} \frac{g_{hSS} g_{hff}}{m_h} \right)^2 \left[ \zeta(6) \left( \frac{T}{m_S} \right)^6 + \frac{\zeta(4)}{180} \left( \frac{m_f}{m_S} \right)^2 \left( \frac{T}{m_S} \right)^4 \right]. \quad (43)$$

Here the transferred momentum  $t$  in the denominator of the amplitude squared is neglected in the calculation consistent with the requirement  $-t < 4|\mathbf{k}|^2 \sim T^2 \ll m_S^2$ . Therefore, for the case with the resulting elastic decoupling temperature  $\sim m_X$  as shown in the left panel of Figs. 3 and 4, the kinetic transition rate should be overestimated, i.e., the true value of  $x_{\text{el}} (\equiv m_X/T_{\text{el}})$  should be less than what is shown (see (iii) in Sec. V for the definition of  $x_{\text{el}}$ ). However, such overestimation does not affect our conclusions.

### 5. The temperature evolution equation for the hidden scalar

After including all interaction terms, we arrive at the Boltzmann moment equation for the temperature of the hidden scalar,

$$\begin{aligned} \frac{dT_S}{dt} + (2 - \delta_H) H T_S = & -(2 - \delta_H) \gamma(T_S - T) - \sum_i \langle \sigma v \rangle_{SS \rightarrow \text{SM}_i \text{SM}_i}(T) \frac{(n_S^{\text{eq}}(T))^2}{n_S(T_S)} (T_S - T) \\ & - \Gamma_S \left( \frac{K_1(x \cdot m_S/m_X)}{K_2(x \cdot m_S/m_X)} (T_S - T \delta_\Gamma(x)) \frac{n_S^{\text{eq}}(T)}{n_S(T_S)} - \frac{K_1(x_S \cdot m_S/m_X)}{K_2(x_S \cdot m_S/m_X)} (1 - \delta_\Gamma(x_S)) T_S \right) \\ & + \frac{(4m_X^2 - m_S^2)(16m_X^2 - m_S^2)}{108m_X(8m_X^2 + m_S^2)} \langle \sigma v^2 \rangle_{XXX \rightarrow XS} \left( \frac{n_X^3(T_S)}{n_S(T_S)} - \frac{n_X(T_S)(n_X^{\text{eq}}(T_S))^2}{n_S^{\text{eq}}(T_S)} \right) \\ & + \frac{(2m_X + 3m_S)(2m_X - m_S)}{6(2m_X + m_S)} \langle \sigma v^2 \rangle_{XXS \rightarrow SS} \left( n_X^2(T_S) - \frac{(n_X^{\text{eq}}(T_S))^2 n_S(T_S)}{n_S^{\text{eq}}(T_S)} \right) \\ & + \frac{m_S(2m_X + m_S)(2m_X + 3m_S)}{4(m_X + 2m_S)(4m_X + 5m_S)} \langle \sigma v^2 \rangle_{XSS \rightarrow XS} \left( n_X(T_S) n_S(T_S) - n_X(T_S) n_S^{\text{eq}}(T_S) \right) \\ & + \frac{5}{54} m_S \langle \sigma v^2 \rangle_{SSS \rightarrow SS} \left( n_S^2(T_S) - n_S(T_S) n_S^{\text{eq}}(T_S) \right), \end{aligned} \quad (44)$$

where

$$\delta_\Gamma(x_i) \equiv \frac{c(T_i)}{m_S^2 T \frac{g_S}{2\pi^2} K_1(x_i \cdot m_S/m_X)}, \quad (45)$$

which approaches 1 in a nonrelativistic  $S$  limit. If considering the temperature below which the DM and hidden scalar are kinetically decoupled, i.e.,  $T_X \neq T_S$ , we need to further include the following two terms to the RHS of Eq. (44),

$$-2\gamma_S(T_S - T_X) + \langle\sigma v\rangle_{XX\rightarrow SS}(T_X) \frac{(n_X(T_X))^2}{n_S(T_S)}(T_X - T_S), \quad (46)$$

where the first and second terms are the kinetic energy-transfer rates by elastic scattering ( $XS \leftrightarrow XS$ ) and by annihilation ( $XX \leftrightarrow SS$ ), respectively. This impact will be discussed in (iv) of Sec. V. Some related results are collected in Appendix D.

By introducing the dimensionless variable,

$$y = \frac{T_S}{T}, \quad (47)$$

the above Boltzmann moment equation for the temperature  $T_S$  can be recasted into an alternative form that will be used in the analysis:

$$\begin{aligned} \frac{dy}{dx} = & - \left( (2 - \delta_H) \frac{\tilde{h}_{\text{eff}}(T)}{h_{\text{eff}}(T)} - 1 \right) \frac{y}{x} - \frac{a}{x^5} \left( \frac{\tilde{h}_{\text{eff}}(T)}{h_{\text{eff}}(T)} \right) \left( \frac{m_X}{m_S} \right)^4 (y - 1) \\ & - \delta_{\text{dof}} \frac{\langle\sigma v\rangle_{SS\rightarrow\sum_i \text{SM}_i \text{SM}_i}(x)}{x^2 \langle\sigma v\rangle_{XX\rightarrow SS}^{(0)}} \frac{(y_S^{\text{eq}}(x))^2}{y_S(x_S)} (y - 1) \\ & - x \frac{\sqrt{90}}{\pi} M_{\text{pl}} \frac{g_*^{1/2}(T)}{h_{\text{eff}}(T)} \frac{\Gamma_S}{m_X^2} \left( \frac{K_1(x \cdot \frac{m_S}{m_X})}{K_2(x \cdot \frac{m_S}{m_X})} \frac{y_S^{\text{eq}}(x)}{y_S(x_S)} (y - \delta_\Gamma(x)) - \frac{K_1(x_S \cdot \frac{m_S}{m_X})}{K_2(x_S \cdot \frac{m_S}{m_X})} (1 - \delta_\Gamma(x_S)) y \right) \\ & + \frac{\delta_{\text{dof}}}{x^4} \frac{\pi}{\sqrt{90}} \frac{h_{\text{eff}}(T)}{g_*^{1/2}(m_X)} \frac{m_X}{M_{\text{pl}}} \\ & \times \left[ \frac{(4m_X^2 - m_S^2)(16m_X^2 - m_S^2)}{108m_X(8m_X^2 + m_S^2)} \frac{\langle\sigma v^2\rangle_{XXX\rightarrow XS}}{(\langle\sigma v\rangle_{XX\rightarrow SS}^{(0)})^2} \left( \frac{y_X^3(x_S)}{y_S(x_S)} - \frac{y_X(x_S)(y_X^{\text{eq}}(x_S))^2}{y_S^{\text{eq}}(x_S)} \right) \right. \\ & + \frac{(2m_X + 3m_S)(2m_X - m_S)}{6(2m_X + m_S)} \frac{\langle\sigma v^2\rangle_{XXS\rightarrow SS}}{(\langle\sigma v\rangle_{XX\rightarrow SS}^{(0)})^2} \left( y_X^2(x_S) - \frac{y_S(x_S)}{y_S^{\text{eq}}(x_S)} (y_X^{\text{eq}}(x_S))^2 \right) \\ & + \frac{m_S(2m_X + m_S)(2m_X + 3m_S)}{4(m_X + 2m_S)(4m_X + 5m_S)} \frac{\langle\sigma v^2\rangle_{XSS\rightarrow XS}}{(\langle\sigma v\rangle_{XX\rightarrow SS}^{(0)})^2} \left( y_X(x_S)y_S(x_S) - y_X(x_S)y_S^{\text{eq}}(x_S) \right) \\ & \left. + \frac{5}{54} m_S \frac{\langle\sigma v^2\rangle_{SSS\rightarrow SS}}{(\langle\sigma v\rangle_{XX\rightarrow SS}^{(0)})^2} \left( y_S^2(x_S) - y_S(x_S)y_S^{\text{eq}}(x_S) \right) \right], \quad (48) \end{aligned}$$

where  $a(m_X/m_S)^4/x^4 \equiv (2 - \delta_H)\gamma/H(T) = (2 - \delta_H)\gamma x^2/H(m_X)$ .

## V. NUMERICAL RESULTS FOR THE THERMAL EVOLUTION OF THE HIDDEN SECTOR

We present the numerical results for thermodynamic evolutions of the normalized yields (proportional to co-moving number densities) and hidden sector temperatures using two sets of masses



for the hidden sector: (i)  $m_X = 80$  GeV,  $m_S = 0.8m_X = 64$  GeV, and (ii)  $m_X = 80$  GeV,  $m_S = 0.99m_X = 79.2$  GeV, where the latter one is the nearly degenerate case. These two sets of the hidden masses are capable of generating one-step cascade DM annihilation spectra that provide a good fit to the observed GC gamma-ray excess which will be further discussed in the next section.

To illustrate this secluded DM model that could be highly decoupled from the SM bath, based these two mass sets, we further take the mixing angle  $\alpha$  to be (1)  $1 \times 10^{-5}$ , (2)  $1 \times 10^{-6}$ , (3)  $5 \times 10^{-7}$ , and (4)  $1 \times 10^{-7}$ , respectively. Meanwhile, in the analysis, we set the parameter  $\lambda_X$ , of which the value is relevant to  $XX \rightarrow SS$  annihilation cross section, to account for the observed DM relic abundance (see Eq. (25)). Our results are shown in Figs. 3 and 4.

The equilibrium number densities, described by the Boltzmann equations given in Eqs. (21) and (22), can be maintained by interactions, including  $XX \leftrightarrow SS$ ,  $SS \leftrightarrow$  SM SM,  $S \leftrightarrow$  SM SM, and  $3 \leftrightarrow 2$  hidden sector cannibalization. The temperature evolution of the hidden scalar is relevant to the kinetic energy transfer by interacting with the bath and with the DM. Such a kinetic energy transfer can be generated from the hidden scalar number changing interactions and from the elastic scattering.

The main results, categorized in terms of temperature scales relevant to the transition phases during the evolution of the hidden sector, are summarized as follows.

- (i)  $x_f \equiv m_X/T_f$  is the usual freeze-out temperature variable. For  $T < T_f$ , the comoving DM number density tend to be conserved. From Eq. (14), we can estimate the freeze-out temperature, below which the DM production rate from  $SS \rightarrow XX$  is overtaken by the dilution rate, giving the relation

$$\langle \sigma v \rangle_{XX \rightarrow SS} \frac{(n_X^{\text{eq}}(T_S))^2}{(n_S^{\text{eq}}(T_S))^2} (n_S(T_S))^2 \lesssim 3H(T)n_X(T_X), \quad (49)$$

where  $T_X = T_S$  before freeze out are functions of  $T$ , and  $T_S$  can be determined by solving numerically the Boltzmann equations, Eqs. (21), (22) and (48). In Figs. 3 and 4,  $x_f$  is denoted by the magenta dot in each plot of the left panel, while the corresponding asymptotic yield  $y_X^\infty$ , described by Eq. (26), is depicted by the horizontal dotted line on the right panel.

For  $T > T_f$ , the rate on the left hand side of Eq. (49) is larger than the expansion rate, resulting in the detailed balance  $\langle \sigma v \rangle_{XX \rightarrow SS}(T_X) (n_X(T_X))^2 = \langle \sigma v \rangle_{SS \rightarrow XX}(T_S) (n_S(T_S))^2$ . This implies that

$$\frac{n_X^2}{(n_X^{\text{eq}})^2} = \frac{n_S^2}{(n_S^{\text{eq}})^2}, \quad (50)$$

so that  $X$  and  $S$  (with  $T_X = T_S$ ) have the same chemical potential,  $\mu_X = \mu_S$ , i.e., the hidden sector is in chemical equilibrium, for which the chemical potential can be non-zero if the hidden scalar undergoes an out-of-equilibrium decay before the DM freezes out (see (vi) for related discussions).

In the right panel of Figs. 3 and 4, the dashed curves exhibit the results with the Boltzmann suppression (i.e., with  $\mu_X = \mu_S = 0$ ) for the hidden sector if  $T_{X,S} = T$ , while dot-dashed curves follow the Boltzmann suppression at their true temperatures, where curves in magenta and blue colors are for the DM and hidden scalar, respectively.

- (ii)  $x_{\text{ann},2} \equiv m_X/T_{\text{ann},2}$ , plotted as the black dot in the left panel of Figs. 3 and 4, corresponds to the bath temperature  $T = T_{\text{ann},2}$  set by

$$(n_S^{\text{eq}}(T))^2 \langle \sigma v \rangle_{SS \rightarrow \sum_i \text{SM}_i \text{SM}_i} T \simeq (2 - \delta_H) H(T) n_S(T_S) T_S, \quad (51)$$

with  $T_S$ , the temperature of  $S$ , being a function of  $T$  determined by Eq. (44). When the bath temperature falls below  $T_{\text{ann},2}$ , the decreasing rate for the kinetic energy density of the hidden scalar due to the expansion of the Universe becomes larger in magnitude than the heating rate transported from the bath via annihilations  $\text{SM SM} \rightarrow SS$ , such that this kind of interactions cannot play the role to keep thermal equilibrium with the SM thermal bath. Here the detailed balance  $\sum_i (n_{\text{SM}_i}^{\text{eq}}(T))^2 \langle \sigma v \rangle_{\text{SM}_i \text{SM}_i \rightarrow SS} = (n_S^{\text{eq}}(T))^2 \langle \sigma v \rangle_{SS \rightarrow \sum_i \text{SM}_i \text{SM}_i}$  has been used. On the other way around, for  $T > T_{\text{ann},2}$ , we have  $T_S \rightarrow T$  (from Eq. (44)), giving that the hidden sector is in thermal equilibrium with the bath.

- (iii)  $x_{\text{el}} \equiv m_X/T_{\text{el}}$ , sketched as the orange dot in the left panel of Figs. 3 and 4, denotes the temperature below which the hidden sector is elastically decoupled from the bath. For  $T > T_{\text{el}}$ , the heating rate of the hidden sector, which gains energy by the elastic scattering  $S \text{ SM} \rightarrow S \text{ SM}$ , is larger in magnitude than the cooling rate due to the Hubble expansion,

$$(2 - \delta_H) \gamma n_S(T_S) T \gtrsim (2 - \delta_H) H(T) n_S(T_S) T_S, \quad (52)$$

where  $(2 - \delta_H) \gamma T$  is the kinetic energy-transfer rate from the relativistic SM particles to a hidden scalar particle via elastic scattering. Unlike the inverse hidden scalar annihilation into relativistic SM particles, of which the rate is depleted through the Boltzmann suppression of the  $S$  number density (with  $\mu_S = 0$ ) for  $T \lesssim m_S$ , the kinetic energy-transfer rate of  $S \text{ SM} \rightarrow S \text{ SM}$  is proportional to the relativistic SM density which is not suppressed. Therefore, in most cases, we have  $x_{\text{el}} > x_{\text{ann},2}$ . Two remarks are in order. First,  $x_{\text{el}} < x_{\text{ann},2}$  may

occur as shown in Fig. 3(a-1) and 3(b-1), if the annihilation cross section is largely enhanced by the resonant  $s$ -channel SM-Higgs exchange with  $s \sim (2m_S)^2 \sim m_h^2$ . Second, compared with the elastic scattering, because the  $2 \rightarrow 2$  annihilation is much more sensitive to  $S$ - $f$ - $\bar{f}$  coupling, which is proportional to  $s_\alpha$ , a small enough mixing angle  $\alpha$  thus results in the  $2 \rightarrow 2$  annihilation decoupling to occur significantly before elastic decoupling. See Figs. 3(d-1) and 4(b-1), 4(c-1), 4(d-1), where  $x_{\text{ann},2}$  is too small to show in some plots.

- (iv)  $x_{\text{de}} \equiv m_X/T_{\text{de}}$  is denoted by a purple “X” in the left panel of Figs. 3 and 4. As seen from Eq. (44), for the hidden scalar particles, when the bath temperature is below  $T_{\text{de}}$ , the heating rate, generated from the inverse decay:  $\text{SM SM} \rightarrow S$ , will be larger in magnitude than that decreased due to expansion of the Universe:

$$\Gamma_S \frac{K_1(x \cdot m_S/m_X)}{K_2(x \cdot m_S/m_X)} n_S^{\text{eq}}(T) \delta_\Gamma T \gtrsim (2 - \delta_H) H n_S(T_S) T_S, \quad (53)$$

where we have used the resulting balance relation,

$$\sum_i \langle \Gamma_{\text{SM}_i \text{SM}_i \rightarrow S} \rangle (n_{\text{SM}_i}^{\text{eq}}(T))^2 = \Gamma_S \frac{K_1(x \cdot m_S/m_X)}{K_2(x \cdot m_S/m_X)} n_S^{\text{eq}}(T). \quad (54)$$

As such, if  $T_{\text{de}} > \min(T_{\text{el}}, T_{\text{ann},2})$  is satisfied, the hidden scalar (as well as the dark matter) can be still maintained in thermal equilibrium with the bath (i.e.,  $n_S(T_S) = n_S^{\text{eq}}(T_S)$  and  $T_S = T$ ) until a later time,  $x_{\text{S,end}} (\equiv m_X/T_{\text{S,end}})$ . In the numerical analysis, we did not include the possible thermal flow due to  $T_S > T_X$  after decoupling. To have a more precise estimate, we know that when the temperature falls below  $T_{\text{S,end}}$ , the heat injected into the hidden scalar particles from the inverse decay  $\text{SM SM} \rightarrow S$  cannot overcome the cooling rate due to Hubble expansion,  $SX \rightarrow SX$  elastic scattering, and  $SS \rightarrow XX$  annihilation, for which the latter two are discussed in Eq. (46) and in Appendix D. Thus the modified  $x_{\text{S,end}}$ , denoted as the blue dot in Figs. 3(a-1), 3(b-1) and 4(a-1), 4(b-1), is determined by

$$\Gamma_S \frac{K_1(x_S \cdot m_S/m_X)}{K_2(x_S \cdot m_S/m_X)} n_S^{\text{eq}}(T_S) T_S \simeq \langle \sigma v \rangle_{XX \rightarrow SS}(T_X) (n_X(T_X))^2 T_S, \quad (55)$$

where the dominant cooling rate from  $SS \rightarrow XX$  annihilation is taken, and the balance relation given in Eq. (54) is used to express the inverse decay rate  $\text{SM SM} \rightarrow S$ . Here  $T_X$  is the DM temperature, and, after DM kinetically decouples from the hidden scalar, satisfies the relation  $T_X = T_X^{\text{kd}} (T/T_X^{\text{kd}})^2$  which is sketched as the red line in the left panel of Figs. 3 and 4, where  $T_X^{\text{kd}} \equiv m_X/x_X^{\text{kd}}$ , depicted as the red dot in Figs. 3(a-1), 3(b-1) and 4(a-1), 4(b-1), is the DM kinetic decoupling temperature, featuring  $T_X^{\text{kd}} \leq T_f$ . A detailed discussion for  $T_X^{\text{kd}}$

will be given in Appendix D. Although the dark matter is out of equilibrium with the hidden scalar, the scalar still receives sufficient kinetic energy from the DM to maintain its thermal equilibrium with the bath for a while, resulting in  $x_{S,\text{end}} \geq x_X^{\text{kd}}$  as shown in Figs. 3(a-1) and 4(a-1). As the mixing angle  $\alpha$  gets smaller, the heating rate from SM  $\text{SM} \rightarrow S$  decreases, so that we have  $x_{S,\text{end}} \rightarrow x_f$  as seen from Figs. 3(b-1) and 4(b-1).

On the other hand, if  $T_{\text{de}} < \min(T_{\text{el}}, T_{\text{ann},2})$  due to a further small decay width of  $S$ , the hidden sector itself in thermal equilibrium can undergo a thermodynamic history having different temperature compared with the SM, but, due to the exponential decay of  $S$ , might be in thermal equilibrium again with the bath at a later time before decoupling; we show the results in Figs. 3(b-1), 3(b-2) and 4(b-1), 4(b-2).

- (v)  $x_c \equiv m_X/T_c$  corresponds to the bath temperature  $T = T_c$ , illustrated by the green dot in the left panel of Figs. 3 and 4 and described by

$$\sum_{i,j,k \equiv S,X} K_{3 \rightarrow 2} \langle \sigma v^2 \rangle_{3 \rightarrow 2} n_i^{\text{eq}}(T_S) n_j^{\text{eq}}(T_S) n_k^{\text{eq}}(T_S) \simeq 2H(T) n_S^{\text{eq}}(T_S) T_S, \quad (56)$$

where  $K_{3 \rightarrow 2}$  shown in Eq. (44) is the kinetic energy released in a relevant  $3 \rightarrow 2$  process involving nonrelativistic  $S$  and  $X$ . For  $T > T_c$ , this number changing interaction maintains the hidden sector, which is undergoing cannibalism, in kinetic equilibrium and in chemical equilibrium with  $\mu_{X,S} = 0$ :  $n_X(T_S) \rightarrow n_X^{\text{eq}}(T_S)$ ,  $n_S(T_S) \rightarrow n_S^{\text{eq}}(T_S)$ . We are interested in the cases, as given in Figs. 3(b), 3(c), 3(d) and 4(b), 4(c), 4(d), that the hidden sector is decoupled from the thermal bath and evolves with different temperature independently, before it becomes nonrelativistic. For these cases with  $T \lesssim m_{S,X}$ , the total comoving entropy density of the hidden sector tends to be conserved before the  $S$  decay occurs. Moreover, during the cannibal process, the entropy density ratio for the SM,  $s_{\text{SM}} = (2\pi^2/45)h_{\text{SM}}^{\text{eff}}(T)T^3$ , to the hidden sector,  $s_h = (2\pi^2/45)h_h^{\text{eff}}(T_S)T_S^3$ , is constant, where  $h_{\text{SM}}^{\text{eff}}$  and  $h_h^{\text{eff}}$  are the effectively relativistic degrees of freedom of the SM and hidden sector, respectively. Thus, we find

$$\frac{T_S}{T} = \left( \frac{s_h}{s_{\text{SM}}} \right)^{1/3} \left( \frac{h_{\text{SM}}^{\text{eff}}(T)}{h_h^{\text{eff}}(T_S)} \right)^{1/3}, \quad (57)$$

where

$$h_h^{\text{eff}}(T_S) \simeq \frac{45}{(2\pi^2)^2} \sum_{h \equiv S,X} g_h \left( \frac{m_h}{T_S} \right)^3 \left[ K_1 \left( \frac{m_h}{T_S} \right) + 4 \frac{T_S}{m_h} K_2 \left( \frac{m_h}{T_S} \right) \right] \quad (\text{for } T_h \lesssim 100 m_X) \quad (58)$$

$$\simeq \frac{45}{2\pi^2} \frac{1}{(2\pi)^{3/2}} \sum_{h \equiv S,X} g_h \left( \frac{m_h}{T_S} \right)^{5/2} e^{-m_h/T_S} \quad (\text{for } T_h \lesssim 0.05 m_X), \quad (59)$$

and  $s_{\text{SM}}/s_h \simeq 30$  for decoupling at  $T \sim m_X$ . From this scenario of entropy conservation, the temperature ratio  $T_h/T$  increases due to cannibalization and follows the dotted gray curve, illustrated on the left panel of Figs. 3 and 4. The hidden sector temperature will deviate from the dotted curve earlier if the out-of-equilibrium decay of  $S$  takes place before the end of cannibalization. As time evolves such that  $T < T_c$ , the cannibal process is inactive, and the out-of-equilibrium number densities of the hidden sector starts to be exponentially depleted (see Figs. 3(c-2), 3(d-2) and 4(c-2), 4(d-2)).

For  $S$  with a lifetime longer than the inverse Hubble rate and during its epoch of cannibalization, the conservation of the total comoving entropy for the hidden sector gives  $s_h a^3 \simeq (\rho_h/T_S) a^3 \simeq \text{constant}$ . Therefore, the comoving number density of hidden sector as well as its temperature decreases logarithmically with the scale factor, i.e. logarithmically with the bath temperature parameter  $x$ ,

$$\frac{m_X n_X + m_S n_S}{s} \sim T_S \sim \frac{m_S}{\log a^3/a_{\text{out,h}}^3} \sim \frac{m_S}{\log x^3/x_{\text{out,h}}^3}, \quad (60)$$

where  $s = s_{\text{SM}} + s_h$ , and  $a_{\text{out,h}}$  (the cosmic scale factor) and  $x_{\text{out,h}}$  (the bath temperature parameter) correspond to the values at which the hidden sector starts to be out of equilibrium with the bath. The logarithmic dependence of the comoving number densities for  $X$  and  $S$  can be seen from Figs. 3(b-2), 3(c-2), 3(d-2) and 4(b-2), 4(c-2), 4(d-2).

- (vi)  $x_{\text{de}}^{\text{out}} \equiv m_X/T_{\text{de}}^{\text{out}}$ , denoted by the purple square in the left panel and by the vertical dashed (red) line in the right panel of Figs. 3 and 4, is the temperature below which the  $S$  decay rate is much larger than its inverse production rate  $\text{SM SM} \rightarrow S$ . Neglecting the logarithmic change of the hidden sector number density due to cannibalization, the normalized yield (proportional to the comoving number density) can be approximated as [31]

$$y_S \simeq 4y_{S,0} e^{-\Gamma_S t}, \quad \text{for } (x_{\text{de}}^{\text{out}})^{-1} \ll (m_X - m_S)/m_X, \quad (61)$$

$$y_S \simeq y_{S,0} e^{-\Gamma_S t/4}, \quad \text{for } m_X \simeq m_S, \quad (62)$$

with

$$t \simeq x^2 \sqrt{\frac{45}{2\pi^2}} \frac{M_{\text{pl}} g_*^{1/2}}{m_X^2 h_{\text{eff}}}, \quad (63)$$

where  $y_{S,0}$  is the normalized yield corresponding to the time after which the hidden sector is decoupled from the thermal bath. When  $x = x_{\text{de}}^{\text{out}}$ , depending on the value of the  $S$  lifetime, we define the yield satisfying  $y_S/y_{S,0} \simeq e^{-1}$ . Note that if the hidden sector exists a cannibal

epoch before freeze-out, a longer-lived  $S$  will result in a larger  $x_f$ , i.e., a larger  $y_X^\infty$ , so that, to have a correct relic density, the dark matter annihilation cross section is generally boosted above the conventional WIMP value. This point will be further discussed in the next section.

For the case that the hidden sector is kinetically decoupled from the bath at  $T \sim m_{X,S}$ , the ending value ( $x_c$ ) of cannibalization depends on the magnitude of  $x_{\text{de}}^{\text{out}}$  since the number density of  $S$  is exponentially depleted during decay. In Figs. 3(d) and 4(d), we show the cases with  $x_{\text{de}}^{\text{out}} \sim x_c$ , for which, when  $S$  decays out of equilibrium, the  $X$  and  $S$  densities are exponentially depleted, instead of following the Boltzmann suppression with a zero chemical potential (see the dot-dashed curves in Figs. 3(d-2) and 4(d-2)). Note that, for this case,  $X$  and  $S$  are still in chemical equilibrium but with non-zero chemical potential before freeze-out. Moreover, it is also interesting to note that for  $T < T_c$ , we have  $T_X = T_S$  and  $T_S = T_S^c \cdot (a^c/a)^2$  even after thermal decoupling, where  $a$  is the cosmic scale factor and  $a^c$  is its corresponding value at  $T_S^c = T_S(T = T_c)$ .

## VI. DISCUSSIONS

Since we have considered the secluded vector dark matter model with DM mass  $\sim \mathcal{O}(80 \text{ GeV})$  as an example to exhibit the thermodynamic evolution of the hidden sector, the related parameters in this model should be very likely constrained by the astrophysical and cosmological measurements. Therefore, before making conclusion, let us discuss the parameter space that can fit to the excess of GeV-scale gamma-rays emitted from the GC region and evade constraints from dwarf spheroidal observation, cosmic microwave background, direct detection, and big bang nucleosynthesis.

The *differential gamma-ray flux* from the one-step cascade DM annihilations is described by

$$\frac{d\Phi_\gamma}{dE} = \frac{\langle\sigma v\rangle_{\text{LV}}}{8\pi m_X^2} \sum_f \text{Br}(S \rightarrow f) \left( \frac{dN_\gamma^f}{dE} \right)_X \underbrace{\frac{1}{\Delta\Omega} \int_{\Delta\Omega} \int_{\text{l.o.s.}} ds \rho^2(r(s, \psi)) d\Omega}_{\text{J-factor}}, \quad (64)$$

where  $\langle\sigma v\rangle_{\text{LV}}$  is the DM annihilation cross section in the low-velocity limit (consistent with  $T \rightarrow 0$ ),  $(dN_\gamma^f/dE)_X$  is the prompt gamma-ray spectrum produced per annihilation with final state  $f$  in the DM rest frame, and the J-factor is the integral along the line of sight (l.o.s.) and over the region of interest (ROI) denoted by the solid angle  $\Delta\Omega$ . We use a Galactic DM density distribution which is a function of  $r$ , the distance to the GC, and parametrized by a generalized Navarro-Frenk-White (gNFW) profile [44, 45],

$$\rho(r) = \rho_\odot \left( \frac{r}{r_\odot} \right)^{-\gamma} \left( \frac{1 + r/r_s}{1 + r_\odot/r_s} \right)^{\gamma-3}, \quad (65)$$

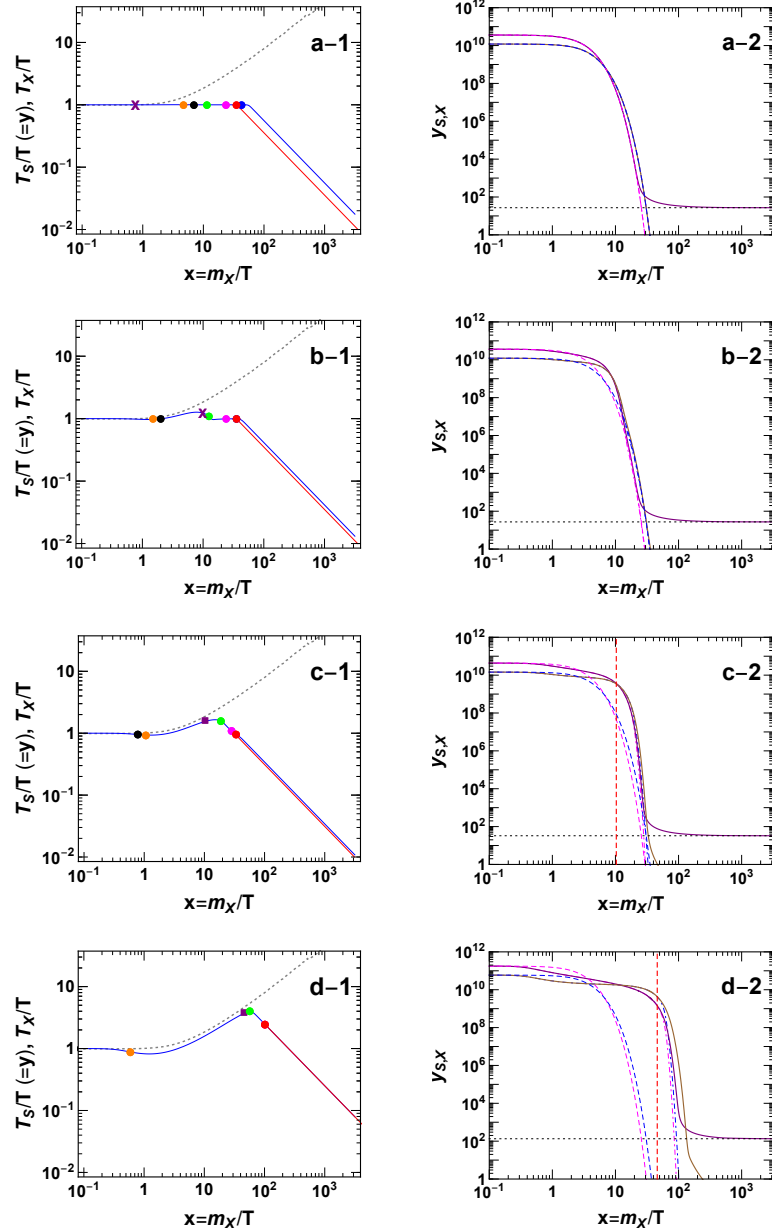


FIG. 3. Left panel:  $T_S/T$  and  $T_X/T$  versus the bath temperature  $T$ . As the DM is decoupled from the hidden scalar,  $T_X/T$  follows the red line. The conservation of the comoving hidden sector entropy is described by the dotted curve (see Eq. (57)). Right panel:  $y_X$  (purple solid line) and  $y_S$  (brown solid line) as functions of  $x$ , where the magenta and blue dashed (or dashed-dotted) lines show the corresponding yields if following Boltzmann suppression with  $T_{S,X} = T$  (or with their true temperatures after decoupling with the bath). The horizontal line denotes the asymptotic DM yield,  $y_X^\infty$ . Here we use  $m_X = 80$  GeV,  $m_S = 64$  GeV, and, in (a), (b), (c), and (d), separately adopt  $\alpha = 1 \times 10^{-5}, 1 \times 10^{-6}, 5 \times 10^{-7}$ , and  $1 \times 10^{-7}$ . The value  $\lambda_X$  is determined to have the correct relic abundance. See the text for details of temperature scales.

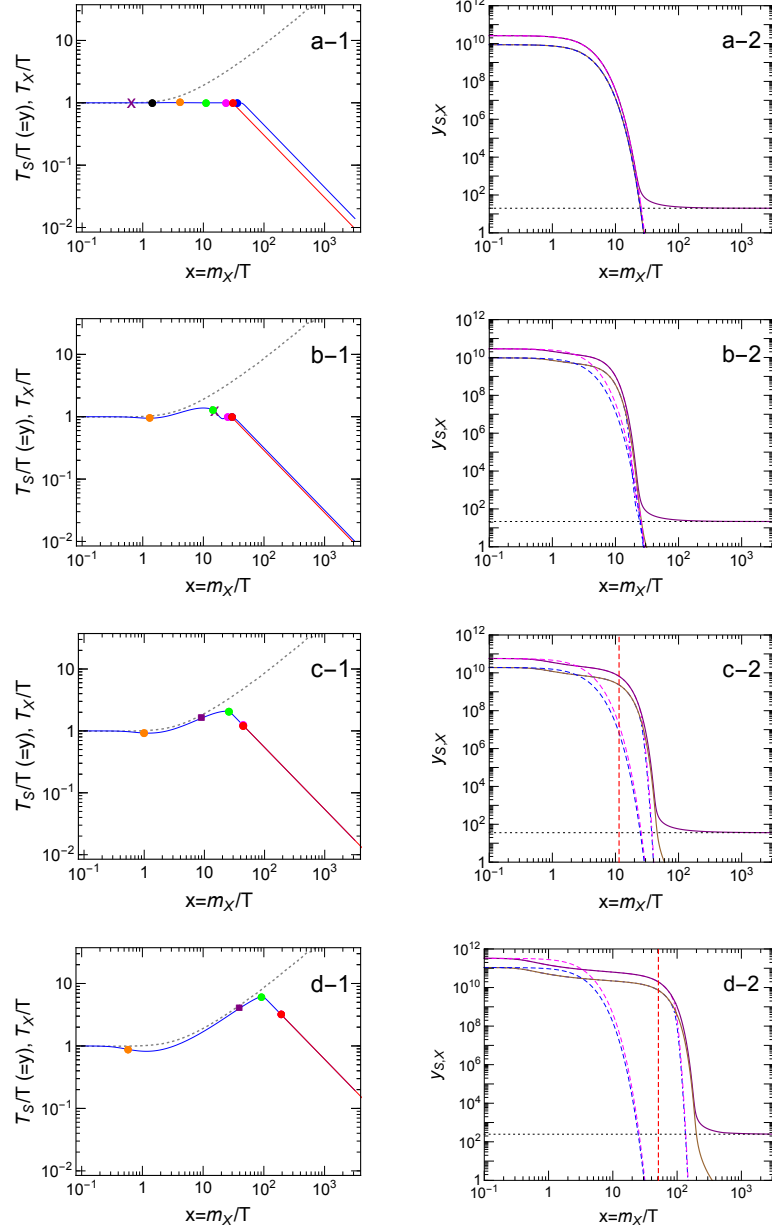


FIG. 4. Same as Fig. 3 but with  $m_X = 80$  GeV and  $m_S = 0.99 m_X$ .

where we adopt  $r_s = 20$  kpc,  $r_\odot = 8.5$  kpc,  $\gamma = 1.2$  and  $\rho_\odot = 0.4$  GeV/cm<sup>3</sup> as the canonical inputs. Here “ $-\gamma$ ” is the inner log slope of the halo density near the GC, and  $\rho_\odot$  is the local DM density at a distance of  $r_\odot$  from the GC. The gamma-ray spectrum in the DM rest frame can be expressed in terms of that given in the rest frame of the metastable mediator ( $S$ ) by means of one-step Lorentz boost [46] (see also Eq. (10) in Ref. [24]), where we use PPC4DMID result [47, 48] to describe the gamma spectra that are generated from the final state SM particle pair in the rest  $S$  decay. As for



the parameter region with  $m_V < m_S < 2m_V$  (with  $V \equiv W$  or  $Z$ ), the three-body decay channel  $S \rightarrow VV^* \rightarrow V f_1 \bar{f}_2$  is kinematically open and becomes much more important when  $m_S$  is close to  $2m_V$  (see also Fig. 1). In the  $S$  rest frame, the gamma-ray spectrum generated from three-body decay channels can be obtained by boosting the gamma-ray spectra produced from the rest  $V$  and from rest  $V^*$ , respectively. Because the description for this part, relevant to the parameter region of the gamma-ray line emission, is sophisticated and does not affect the conclusion of this paper, we will thus defer the details in a future study.

Using the GC excess result extracted by Calore, Cholis, and Weniger (CCW) [8] from the study of Fermi-LAT Pass 7 data, where the gamma-ray spectrum covers the energy range between 300 MeV to 500 GeV in the  $40^\circ \times 40^\circ$  square ROI around the Galactic center with latitude  $|b| \leq 2^\circ$  masked out, we do the goodness-of-fit with a  $\chi^2$  test statistic for the DM mass and annihilation cross section  $\langle\sigma v\rangle_{LV}$ . In Fig. 5, two ratio values of  $m_S = 0.8m_X$  and  $m_S = 0.99m_X$  are used to show the GC excess result, where, taking  $\rho_\odot = 0.4 \text{ GeV/cm}^3$  and  $\gamma = 1.2$ , the blue regions with solid, dashed and dotted boundaries respectively satisfy p-value  $\geq 0.3$ , 0.15, and 0.05, corresponding to  $\chi^2/\text{dof} = 24.9/22$ , 28.8/22, and 33.9/22. The best fit is denoted as the blue dot with p-value = 0.46 or 0.42, corresponding to  $\chi^2_{\min}/\text{dof} = 22.0/22$  or 22.7/22, for the case of  $m_S = 0.8m_X$  or  $m_S = 0.99m_X$ .

Further allowing variation of  $\rho_\odot \in [0.2, 0.6] \text{ GeV/cm}^3$  and  $\gamma \in [1.1, 1.3]$ , the value of  $\langle\sigma v\rangle_{LV}$  can be raised (or lowered) extremely by a factor of 2.94 (or 0.194). For illustration, in Fig. 5, we also show the GC allowed region in orange color corresponding to  $\rho_\odot = 0.6 \text{ GeV/cm}^3$  and  $\gamma = 1.3$ , while that in pink color corresponding to  $\rho_\odot = 0.2 \text{ GeV/cm}^3$  and  $\gamma = 1.1$ . In Fig. 6, the GC fit together with other constraints is redrawn on the  $(m_X, \lambda_X)$  plane, where a larger  $\lambda_X$  is needed to account for the data for the nearly degenerate case because  $\langle\sigma v\rangle_{LV}$  vanishes in the limit  $m_S \rightarrow m_X$ .

We remark that a newer Pass 8 Fermi data set was analyzed in Ref. [49], in which the authors showed that the considerable difference between Fermi Pass 7 and Pass 8 data appears only at low energies which might be due to the modeling for the point sources in various datasets [11, 49].

In Fig. 5, the relic density of the conventional WIMP dark matter is accounted for by the narrow gray range, while above the gray range the nonconventional WIMP scenario, showing a boosted annihilation cross section, can be satisfied. The result can be also easily read from Fig. 7, where the nonconventional WIMP scenario corresponds to a small mixing angle  $\alpha \lesssim 2 \times 10^{-6}$ , for which the hidden sector has kinetically decoupled from the thermal bath before it becomes nonrelativistic. The resulting nonconventional WIMP DM annihilation cross section that can account for the correct relic density is significantly boosted above the conventionally thermal WIMP value for

$\alpha \lesssim 6 \times 10^{-7}$  (or  $\alpha \lesssim 1 \times 10^{-6}$ ) if  $m_X = 80$  GeV,  $m_S = 64$  GeV (or  $m_X = 80$  GeV,  $m_S = 79.2$  GeV).

Fig. 5 shows constraints from the Fermi gamma-ray observations of dwarf spheroidal galaxies (dSphs) and the measurement of the cosmic microwave background (CMB). For the dSphs constraint, we have performed a combined likelihood analysis using the 6-year Fermi-LAT data of 28 confirmed and 17 candidate dSphs for gamma-ray energies within 500 MeV to 500 GeV [50, 51]. In the likelihood analysis, we adopt the spectroscopically determined nominal J-factor for the individual target along with its error when possible, or use a predicted value from the distance scaling relationship with an uncertainty of 0.6 dex, otherwise [50]. See the detailed description in Ref. [31] for the likelihood analysis. We also show the dSphs projection sensitivity denoted by the dashed red line by assuming that the 15-year data can be collected from 60 dSphs. For the CMB constraint which is complementary to that determined from dSphs observations, the Planck set a bound from temperature and polarization data (TT, TE, EE+lowP) at recombination to be [26]

$$f_{\text{eff}}(m_X) \frac{\langle \sigma v \rangle_{\text{CMB}}}{m_X} < 4.1 \times 10^{-28} \text{ cm}^3 \text{s}^{-1} \text{GeV}^{-1}, \quad (66)$$

where  $\langle \sigma v \rangle_{\text{CMB}} \simeq \langle \sigma v \rangle_{\text{LV}}$  for s-wave DM annihilation, and the efficiency factor is

$$f_{\text{eff}}(m_X) = \frac{1}{2m_X} \int_0^{m_X} E dE \left[ 2f_{\text{eff}}^{e^-}(E) \left( \frac{dN_{e^-}}{dE} \right)_X + f_{\text{eff}}^{\gamma}(E) \left( \frac{dN_{\gamma}}{dE} \right)_X \right]. \quad (67)$$

Here, we use  $f_{\text{eff}}^{\gamma, e^-}(E)$  curve results suited for the “3 keV” baseline prescription shown in Ref. [52]. Moreover, as the previous study for the GC excess,  $(dN_{\gamma, e^-}/dE)_X$  generated from the one-step cascade DM annihilation is the photon/electron energy spectrum that can be obtained by boosting the spectra provided in PPPC4DMID. The current bound obtained from the CMB analysis seems to be much weaker than that from the Fermi-LAT dSphs data (see also Fig. 7).

In order to have a more comprehensive understanding of the phenomenological constraints on the secluded DM that could exhibit a boosted DM annihilation cross section, as discussed in the previous section, using the two ratio values of  $m_S = 0.8m_X$  and  $m_S = 0.99m_X$  with  $m_X = 80$  GeV, we display the correct relic abundance as the black curve on the  $(\alpha, x_f)$  plane in Fig. 7, where for  $\alpha$  the corresponding values of  $S$  decay width  $\Gamma_S$  is depicted, while for  $x_f$  the related  $y_X^\infty$ ,  $\langle \sigma v \rangle_{\text{LV}}$  and  $\langle \sigma v \rangle_{T_f}$  are indicated. The range favored by observed features of the GC excess with variation of  $\rho_\odot \in [0.2, 0.6] \text{ GeV/cm}^3$  and  $\gamma \in [1.1, 1.3]$  is given in between the two horizontal dot-dashed (purple) lines.

As shown in Fig. 7, the LZ projected sensitivity can only reach the RHS of the dotted (blue) curve corresponding to the thermal WIMP region with  $\alpha \gtrsim 3.7 \times 10^{-3}$  for  $(m_X, m_S) = (80 \text{ GeV}, 64 \text{ GeV})$ , or for  $\alpha \gtrsim 5.5 \times 10^{-3}$  for  $(m_X, m_S) = (80 \text{ GeV}, 79.2 \text{ GeV})$ . If  $\alpha$  is larger than the

value denoted by the vertical dashed (magenta) line which corresponds to  $T_{\text{de}} = \min(T_{\text{el}}, T_{\text{ann},2})$ , the hidden sector particles can be well in the chemical and thermal equilibrium with the bath before freeze out. Nevertheless, the case of  $(m_X, m_S) = (80 \text{ GeV}, 64 \text{ GeV})$  with  $\alpha \lesssim 6 \times 10^{-7}$ , or  $(m_X, m_S) = (80 \text{ GeV}, 79.2 \text{ GeV})$  with  $\alpha \lesssim 1 \times 10^{-6}$ , clearly exhibits the boosted annihilation cross section capable of accounting for the correct relic density. The 95% C.L. limit from CMB is denoted as the dot-dashed (brown) line, while the 95% C.L. limit and project sensitivity for dSphs observations are shown as horizontal solid (red) and long-dashed (red) lines, respectively. The boosted annihilation cross section is thus stringently constrained by the current dSphs observations. The secluded DM scenario can be further tested by the dSphs projection.

Finally, we discuss the bound on the lifetime of the hidden scalar from the big bang nucleosynthesis constraint, i.e., a lower bound on the mixing coupling  $\alpha$ . If the hidden scalar survives with a longer lifetime  $\tau_S \gtrsim 0.01s$ , the deficit of the neutrino distribution functions due to the insufficient thermalization will result in increasing deviation of  $N_{\text{eff}}$  from three and become smaller [53], where  $N_{\text{eff}}$  is the effective number of the neutrino species, characterizing the evolution of energy density of three neutrino species. Combining CMB observations with baryon acoustic oscillation data, Planck reported the result  $N_{\text{eff}} = 3.15 \pm 0.23$  [26], from which we can impose the constraint  $\tau_S \lesssim 0.02s$  [53]. As such, we have  $\alpha \gtrsim 1.4 \times 10^{-10}$  for  $(m_X, m_S) = (80 \text{ GeV}, 64 \text{ GeV})$ , or  $\alpha \gtrsim 1.2 \times 10^{-10}$  for  $(m_X, m_S) = (80 \text{ GeV}, 79.2 \text{ GeV})$ .

## VII. CONCLUSIONS

Using the secluded vector dark matter model, we have presented a comprehensive study on thermodynamic evolutions of the hidden sector particles from the first principle. We have solved numerically the coupled Boltzmann moment equations for number densities and temperature evolutions of the hidden sector particles. Our formalism can be easily extended to a general secluded dark matter model.

Taking two mass sets: (i)  $m_X = 80 \text{ GeV}$ ,  $m_S = 0.8m_X = 64 \text{ GeV}$ , and (ii)  $m_X = 80 \text{ GeV}$ ,  $m_S = 0.99m_X = 79.2 \text{ GeV}$ , we have shown the detailed thermodynamics for which, while the dark matter in thermal equilibrium with the hidden scalar is secluded from the visible sector with small interaction rates generated from the direct detection and collider experiments, the hidden sector can be either in thermal equilibrium or out of equilibrium with the bath before the DM freezes out. The results are briefly summarized as below. More details about the thermodynamics of the hidden sector have been given in Sec. V.

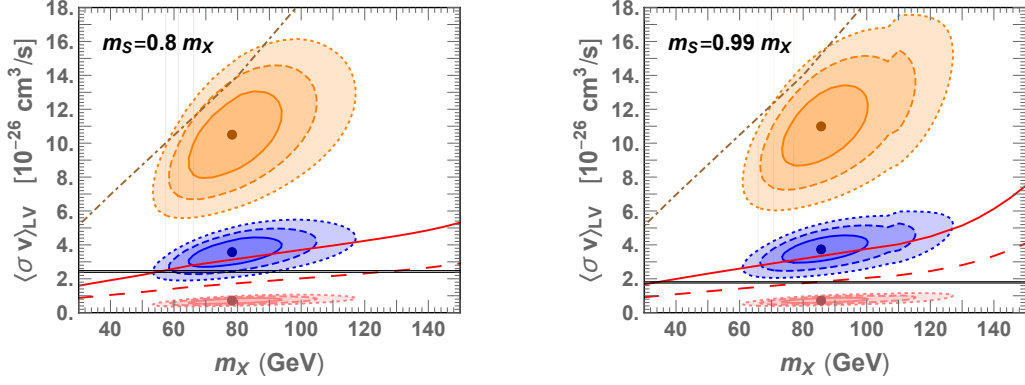


FIG. 5. The GC allowed regions in the dark matter mass  $m_X$  and low-velocity annihilation cross section  $\langle\sigma v\rangle_{LV}$  plane, where the best-fit point is denoted as the dot, and the regions with solid, dashed and dotted boundaries, satisfy  $p$ -value  $\geq 0.3$ ,  $0.15$ , and  $0.05$ , respectively. The regions with color to be blue, orange, and pink refer to  $(\rho_\odot, \gamma) = (0.4 \text{ GeV/cm}^3, 1.2)$ ,  $(0.6 \text{ GeV/cm}^3, 1.3)$ , and  $(0.2 \text{ GeV/cm}^3, 1.1)$ . In conventional WIMP DM, the relic density is accounted for by the narrow gray range, while for the nonconventional WIMP, the allowed relic density could be extended to the upper region of the gray range. The 95% C.L. upper bound and projected limit from Fermi-LAT observations of dSphs are denoted as the solid and long-dashed red lines, respectively, while the Planck CMB 95% C.L. upper limit is depicted as dot-dashed brown line.

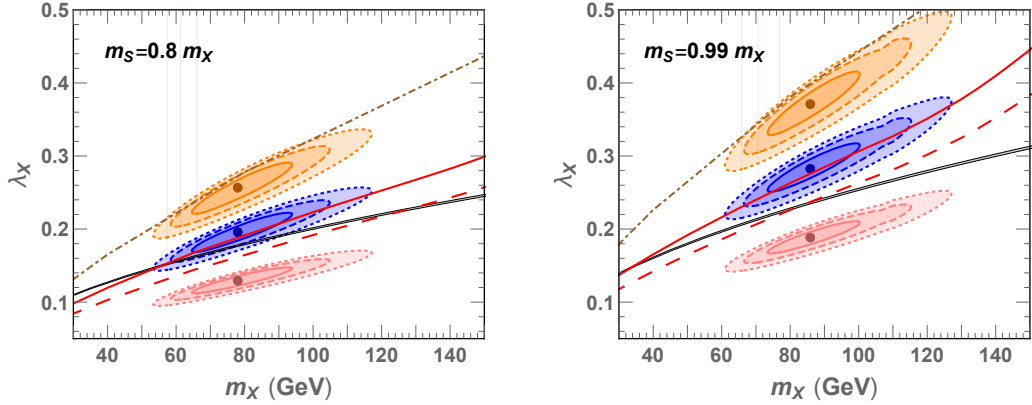


FIG. 6. Same as Fig. 5, but in the  $(m_X, \lambda_X)$  plane.

For the case satisfying  $T_{\text{de}} \geq \min(T_{\text{el}}, T_{\text{ann},2})$ , the kinetic decoupling of elastic scattering  $S \text{ SM} \leftrightarrow S \text{ SM}$  and/or annihilation  $SS \leftrightarrow \text{SM SM}$  occurs only when the bath temperature is below  $T_{\text{de}}$  at which the heating rate of the hidden sector generated from the inverse decay  $\text{SM SM} \rightarrow S$  starts to overcome the dilution rate due to the cosmic expansion. As such, the nonrelativistic hidden sector can keep thermal equilibrium with the bath until freeze-out. Therefore, the DM is consistent with

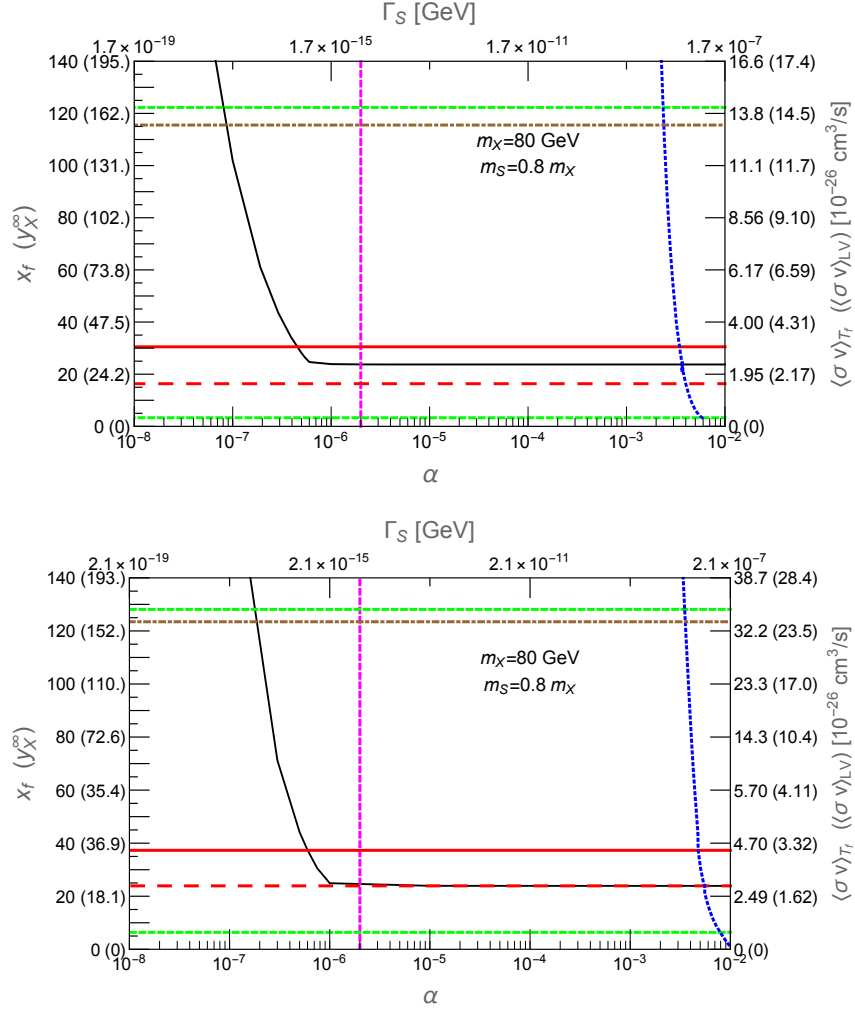


FIG. 7.  $x_f$  as a function of  $\alpha$ , denoted as the black curve that reproduces the correct relic abundance, where for the former the corresponding thermally averaged DM annihilation cross section at  $T_f$  is given, and for the latter the resulting  $S$  decay width  $\Gamma_S$  is illustrated. The corresponding values of  $y_X^\infty$  and the low-velocity DM annihilation cross section are also depicted. The 95% C.L. upper limit from CMB is denoted as the dot-dashed (brown) line. The 95% C.L. upper limit and project sensitivity for dSphs observations are shown as horizontal solid (red) and long-dashed (red) lines, respectively. The RHS of the dotted (blue) curve corresponds to projected reach by LZ. When  $\alpha$  is larger than that denoted by the vertical dashed (magenta) line, the dark sector is in the chemical thermal equilibrium with the bath before freeze out. The region between the two horizontal short-dashed (green) lines provides a good fit to the GC gamma-ray excess.

the conventional WIMP scenario, but can easily evade the searches from the colliders and direct detections (*e.g.* projected LZ measurement) for a small mixing angle  $2 \times 10^{-6} \lesssim \alpha \lesssim 4 \times 10^{-3}$  as in the present model.

On the other hand, for the case that the hidden sector starts to be kinetically decoupled from

the thermal bath at  $T \sim m_{X,S}$  due to its weak couplings to the SM particles, the nonrelativistic hidden sector will first undergo a cannibal epoch, during which the total comoving entropy density of the hidden sector is approximately conserved before  $S$  decays out of equilibrium. When out-of-equilibrium  $S$  decay occurs, the hidden sector particles  $X$  and  $S$  are still in chemical equilibrium, but their densities, instead of following Boltzmann suppression with zero chemical potential, are exponentially depleted with non-zero chemical potential until freeze-out. We have shown that having a small mixing angle  $\alpha \lesssim 6 \times 10^{-7}$  (or  $\alpha \lesssim 1 \times 10^{-6}$ ) which corresponds to  $m_X = 80$  GeV,  $m_S = 64$  GeV (or  $m_X = 80$  GeV,  $m_S = 79.2$  GeV), the secluded DM annihilates into “long-lived” hidden mediators which later decay out of equilibrium with the bath, such that the resulting nonconventional WIMP-like DM annihilation cross section accounting for the observed relic density is boosted above the conventionally thermal WIMP value.

For the experimental constraints, we have shown the parameter space which yields a good fit to the GC excess data and is compatible with the LZ projected sensitivity, BBN bound, Planck CMB measurement and Fermi dSphs observation. Moreover, we expect that Fermi-LAT 15-yr dSph observations can explore the parameter region of the correct relic density described not only by the nonconventional WIMP scenario but also, if the DM and hidden scalar are not well degenerate, by the conventional WIMP one.

## ACKNOWLEDGMENTS

This work was supported in part by the Ministry of Science and Technology, Taiwan, under Grant No. 105-2112-M-033-005.

## Appendix A: The partial decay widths of the hidden mediator $S$

The main partial decay widths of the hidden scalar  $S$  with mass  $\lesssim 130$  GeV are given by

$$\Gamma(S \rightarrow \bar{f}f) = K_f N_c^f \frac{m_S}{8\pi} g_{Sff}^2 \left(1 - \frac{4m_f^2}{m_S^2}\right)^{3/2} \theta(m_S - 2m_f), \quad (\text{A1})$$

$$\Gamma(S \rightarrow gg) = K_g \frac{\alpha_s^2}{2\pi^3 m_S} \left| \sum_{q \equiv \text{quark}} m_q g_{Sq} f_S \left( \frac{4m_q^2}{m_S^2} \right) \right|^2, \quad (\text{A2})$$

$$\Gamma(S \rightarrow VV^*) = \frac{3G_F^2 m_V^4}{16\pi^3} m_S s_\alpha^2 \delta'_V R_T(x) \theta(m_S - m_V), \quad (\text{A3})$$

where  $N_c^{q(\ell)} \equiv 3(1)$  for the quark (lepton),  $G_F = (\sqrt{2}v_H^2)^{-1}$ , the coupling  $g_{Sff} = -s_\alpha m_f/v_H$ ,  $K_q = 1 + 5.67\alpha_s(\mu)/\pi$  and  $K_g = 1 + (215/12)\alpha_s(\mu)/\pi$  are the NLO QCD corrections [54],  $\delta'_W = 1$ ,

$$\delta'_Z = \frac{7}{12} - \frac{10}{9} \sin^2 \theta_W + \frac{40}{27} \sin^4 \theta_W,$$

$$R_T(x) = \frac{3(1-8x+20x^2)}{(4x-1)^{1/2}} \arccos\left(\frac{3x-1}{2x^{3/2}}\right) - \frac{1-x}{2x}(2-13x+47x^2) - \frac{3}{2}(1-6x+4x^2) \log x,$$

with  $x \equiv m_V^2/m_S^2$  [55, 56], and  $f_S(\tau) = [1 + (1-\tau)f(\tau)]$  with

$$f(\tau) = \begin{cases} \arcsin^2 \sqrt{\tau-1}, & \tau \geq 1 \\ -\frac{1}{4} \left[ \log \frac{1+\sqrt{1-\tau}}{1-\sqrt{1-\tau}} - i\pi \right]^2, & \tau < 1 \end{cases}. \quad (\text{A4})$$

Here, we will take the scale  $\mu = m_S/2$ .

## Appendix B: $2 \rightarrow 2$ annihilation cross sections

### 1. The annihilation process for $XX \rightarrow SS$

In this secluded DM case, the relic density is determined by the thermally averaged annihilation cross section  $\langle \sigma v_{\text{Mø}} \rangle_{XX \rightarrow SS}$  which is also relevant to the indirect detection searches, where  $v_{\text{Mø}}$  is the Møller velocity. The value of  $\langle \sigma v_{\text{Mø}} \rangle_{XX \rightarrow SS}$  equals to  $\langle \sigma v_{\text{lab}} \rangle_{XX \rightarrow SS}$  which is the result calculated in the rest frame of one of the incoming particles.

The diagrams for the  $XX \rightarrow SS$  process are depicted in Fig. 8, where the  $s$ -channel annihilation via  $h$  is negligible and does not shown. The resulting cross section is given by

$$\begin{aligned} & (\sigma v_{\text{lab}})_{XX \rightarrow SS} \\ &= \frac{c_\alpha^2 \lambda_X^2 \sqrt{s-4m_S^2}}{288\pi m_X^4 \sqrt{s}(s-2m_X^2)((s-m_S^2)^2 + \Gamma_S^2 m_S^2)} \times \left[ \frac{2c_\alpha^2 \lambda_X^2 ((s-m_S^2)^2 + \Gamma_S^2 m_S^2)}{m_S^4 - 4m_S^2 m_X^2 + m_X^2 s} \right. \\ & \times \left( 3m_S^8 - 20m_S^6 m_X^2 + m_S^4 (46m_X^4 + 6m_X^2 s) - 4m_S^2 (14m_X^6 + 5m_X^4 s) + 48m_X^8 + 6m_X^6 s + 4m_X^4 s^2 \right) \\ & + g_{SSS}^2 m_X^2 (12m_X^4 - 4m_X^2 s + s^2) - 4g_{SSS} c_\alpha \lambda_X m_X (m_S^2 - s)(m_S^2 (2m_X^2 + s) - m_X^2 (6m_X^2 + s)) \\ & - \frac{8c_\alpha \lambda_X \text{Arcoth}\left(\frac{s-2m_S^2}{\sqrt{s-4m_S^2}\sqrt{s-4m_X^2}}\right)}{(s-2m_S^2)\sqrt{s-4m_S^2}\sqrt{s-4m_X^2}} \left( c_\alpha \lambda_X ((s-m_S^2)^2 + \Gamma_S^2 m_S^2) \right. \\ & \times \left( 3m_S^8 - 2m_S^6 (6m_X^2 + s) + 2m_S^4 (4m_X^4 + 5m_X^2 s) - 4m_S^2 m_X^2 (4m_X^4 + s^2) + 24m_X^6 (s-2m_X^2) \right) \\ & \left. \left. - g_{SSS} m_X (s-2m_S^2)(s-m_S^2) (m_S^2 (2m_X^2 + s)(m_S^2 - 4m_X^2) + 2m_X^2 (12m_X^4 - 2m_X^2 s + s^2)) \right) \right], \quad (\text{B1}) \end{aligned}$$

where  $s$  is the center-of-mass energy squared, and

$$g_{SSS} = -\frac{3c_\alpha^3 m_S^2}{v_S} + \frac{3s^3 m_S^2}{v_H}. \quad (\text{B2})$$

Using the above result, the thermally averaged annihilation cross section for  $T \lesssim 3m_X$  can be obtained by calculating [57],

$$\langle \sigma v_{\text{lab}} \rangle_{XX \rightarrow SS} = \frac{1}{8m_X^4 T K_2^2(m_X/T)} \int_{4m_X^2}^{\infty} (\sigma v_{\text{lab}})_{XX \rightarrow SS} (s - 2m_X^2)(s - 4m_X^2)^{1/2} K_1(\sqrt{s}/T) ds, \quad (\text{B3})$$

with  $K_{1,2}$  being the modified Bessel functions. At the indirect detection, we can take the approximation in the low-velocity limit, i.e.,  $\langle \sigma v_{\text{lab}} \rangle_{XX \rightarrow SS} = (\sigma v_{\text{lab}})_{XX \rightarrow SS}$  with the replacement  $s = 4m_X^2$ .

## 2. The annihilation process for $SS \rightarrow \text{SM SM}$

The diagrams for the hidden scalar  $S$  annihilation into the SM particles are depicted in Fig. 9. The resulting annihilation cross section is given by

$$\begin{aligned} (\sigma v_{\text{lab}})_{SS \rightarrow \bar{f}f} = & N_c^f \frac{\sqrt{s - 4m_f^2}}{8\pi\sqrt{s}(s - 2m_S^2)} \left( \frac{g_{Sff}^2 g_{SSS}^2 (s - 4m_f^2)}{(s - m_S^2)^2 + \Gamma_S^2 m_S^2} + \frac{g_{hSS}^2 g_{hff}^2 (s - 4m_f^2)}{(s - m_h^2)^2 + \Gamma_h^2 m_h^2} \right. \\ & + \frac{2g_{Sff}^4 (m_f^2 (4s - 8m_S^2) + 2m_f^4 - 4m_S^2 s + s^2) \ln \left( \frac{s - 2m_S^2 + \sqrt{s - 4m_f^2} \sqrt{s - 4m_S^2}}{s - 2m_S^2 - \sqrt{s - 4m_f^2} \sqrt{s - 4m_S^2}} \right)}{\sqrt{s - 4m_f^2} \sqrt{s - 4m_S^2} (s - 2m_S^2)} \\ & + \frac{2g_{SSS} g_{hSS} g_{Sff} g_{hff} (s - 4m_f^2) (\Gamma_h \Gamma_S m_h m_S + (m_h^2 - s)(m_S^2 - s))}{((s - m_h^2)^2 + \Gamma_h^2 m_h^2) ((s - m_S^2)^2 + \Gamma_S^2 m_S^2)} \\ & - \frac{4g_{Sff}^3 g_{SSS} m_f \sqrt{s - 4m_f^2} (s - m_S^2) \ln \left( \frac{s - 2m_S^2 + \sqrt{s - 4m_f^2} \sqrt{s - 4m_S^2}}{s - 2m_S^2 - \sqrt{s - 4m_f^2} \sqrt{s - 4m_S^2}} \right)}{\sqrt{s - 4m_S^2} ((s - m_S^2)^2 + \Gamma_S^2 m_S^2)} \\ & + \frac{4g_{Sff}^2 g_{hSS} g_{hff} m_f \sqrt{s - 4m_f^2} (m_h^2 - s) \ln \left( \frac{s - 2m_S^2 + \sqrt{s - 4m_f^2} \sqrt{s - 4m_S^2}}{s - 2m_S^2 - \sqrt{s - 4m_f^2} \sqrt{s - 4m_S^2}} \right)}{\sqrt{s - 4m_S^2} ((s - m_h^2)^2 + \Gamma_h^2 m_h^2)} \\ & \left. - \frac{2g_{Sff}^4 (8m_f^4 - 4m_f^2 m_S^2 + m_S^4)}{m_f^2 (s - 4m_S^2) + m_S^4} \right), \quad (\text{B4}) \end{aligned}$$

where  $N_c^f \equiv 3(1)$  for  $f \equiv$  quarks (leptons),  $g_{SSS}$  is shown in Eq. (B2), and the remaining couplings are

$$g_{hSS} = -\frac{c_\alpha^2 s_\alpha (2m_S^2 - m_h^2)}{v_S} - \frac{c_\alpha s_\alpha^2 (2m_S^2 - m_h^2)}{v_H}, \quad (\text{B5})$$

$$g_{hff} = \frac{m_f}{v_H} c_\alpha, \quad (\text{B6})$$

$$g_{Sff} = \frac{m_f}{v_H} s_\alpha. \quad (\text{B7})$$



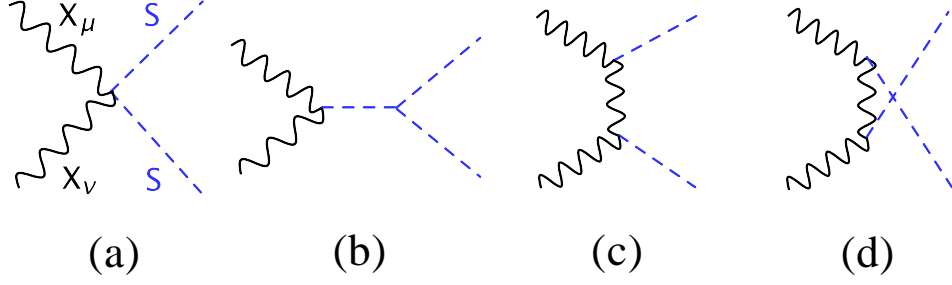


FIG. 8. Feynman diagrams that dominantly contribute to the DM annihilation cross section.

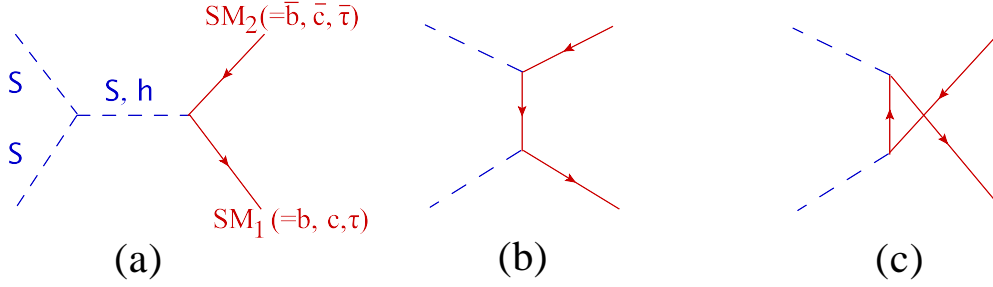


FIG. 9. Feynman diagrams for the annihilation of the hidden scalar pair into SM particles. The results are relevant to the chemical equilibrium between the hidden sector and thermal bath in the early Universe.

On can further apply Eq. (B3) to obtain thermally averaged value of the annihilation cross section. This result is relevant to the chemical equilibrium between the hidden sector and thermal bath in the early Universe.

### Appendix C: $3 \rightarrow 2$ annihilations

We consider a thermally averaged cannibal annihilation cross section for  $a(p_a) b(p_b) c(p_c) \rightarrow d(p_d) e(p_e)$ , where all particles resides in a hidden sector and keep the same temperature,  $T_X = T_S = T_h$ , during the interaction. The generic form defined through this paper is given by

$$\begin{aligned} \langle \sigma v^2 \rangle(T_h) &= \frac{1}{m!} \frac{1}{n_a^{\text{eq}}(T_h) n_b^{\text{eq}}(T_h) n_c^{\text{eq}}(T_h)} \int \frac{d^3 p_a}{(2\pi)^3 2E_a} \frac{d^3 p_b}{(2\pi)^3 2E_b} \frac{d^3 p_c}{(2\pi)^3 2E_c} \frac{d^3 p_d}{(2\pi)^3 2E_d} \frac{d^3 p_e}{(2\pi)^3 2E_e} \\ &\quad \times (2\pi)^4 \delta^{(4)}(p_a + p_b + p_c - p_d - p_e) |M|_{abc \rightarrow de}^2 e^{-(E_a + E_b + E_c)/T_h} \\ &= \frac{1}{n_a^{\text{eq}}(T_h) n_b^{\text{eq}}(T_h) n_c^{\text{eq}}(T_h)} \int \frac{d^3 p_a}{(2\pi)^3 2E_a} \frac{d^3 p_b}{(2\pi)^3 2E_b} \frac{d^3 p_c}{(2\pi)^3 2E_c} \sigma v^2 e^{-(E_a + E_b + E_c)/T_h}, \quad (\text{C1}) \end{aligned}$$

where  $m \equiv 2$  if the final state particles,  $d$  and  $e$ , are the same particle species, otherwise  $m \equiv 1$ . Here, the sum for the amplitude squared,  $|M|_{abc \rightarrow de}^2$ , has been taken over all internal degrees of

freedom of the initial and final states. In the nonrelativistic limit,  $E_a \approx m_a, E_b \approx m_b, E_c \approx m_c$ , the cross section is approximately given by [30]

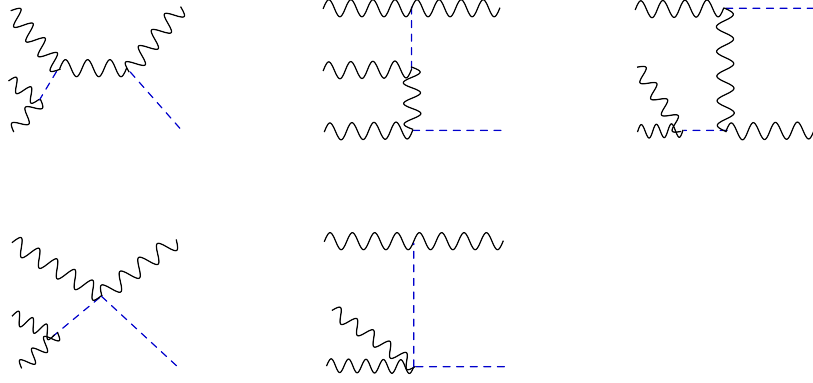
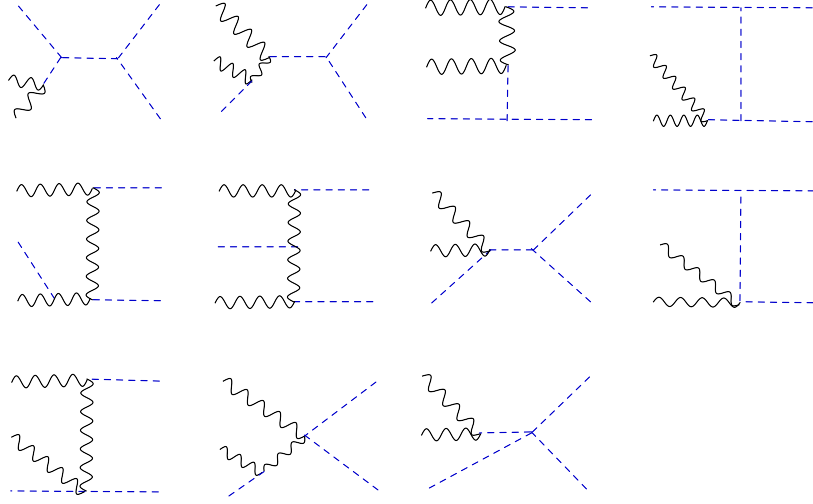
$$\sigma v^2 = \frac{[(m_a + m_b + m_c)^4 - 2(m_a + m_b + m_c)^2(m_d^2 + m_e^2) + (m_d^2 - m_e^2)^2]^{1/2}}{m! 64 \pi m_a m_b m_c (m_a + m_b + m_c)^2} |M|_{abc \rightarrow de}^2. \quad (C2)$$

To calculate  $3 \rightarrow 2$  thermally averaged annihilation cross sections for the nonrelativistic hidden sector particles with a temperature below their masses, i.e.,  $T_h < m_{S,X}$ , we take the low-velocity approximation,  $\langle \sigma v^2 \rangle \simeq \sigma v^2$  and neglect its subleading corrections of order  $T_h/m_{X,S}$ . We show the diagrams in Figs. 10, 11, 12, 13, and 14, and summarize all the relevant results as below,

$$\begin{aligned} \langle \sigma v^2 \rangle_{XXX \rightarrow XS} &\simeq \frac{[(16m_X^2 - m_S^2)(4m_X^2 - m_S^2)]^{1/2}}{1152\pi m_X^7} 2\lambda_X^6 m_X^2 \\ &\times \left( \frac{m_S^4}{12m_X^6} - \frac{19m_S^2}{6m_X^4} + \frac{2773}{36m_X^2} + \frac{1620}{m_S^2 + 2m_X^2} - \frac{2916m_S^2}{(m_S^2 + 2m_X^2)^2} + \frac{27m_S^2}{64(2m_X - m_S)^4} \right. \\ &+ \frac{27m_S^2}{64(m_S + 2m_X)^4} - \frac{18237}{128m_S(2m_X - m_S)} + \frac{18237}{128m_S(m_S + 2m_X)} \\ &\left. - \frac{7683}{128(2m_X - m_S)^2} - \frac{7683}{128(m_S + 2m_X)^2} - \frac{213m_S}{8(2m_X - m_S)^3} + \frac{213m_S}{8(m_S + 2m_X)^3} \right), \end{aligned} \quad (C3)$$

$$\begin{aligned} \langle \sigma v^2 \rangle_{XSS \rightarrow SS} &\simeq \frac{[(2m_X - m_S)(2m_X + 3m_S)]^{1/2}}{128\pi m_X^4 m_S(2m_X + m_S)} \lambda_X^6 m_X^2 \\ &\times \left( \frac{1971m_S^2}{16m_X^4} + \frac{172m_S^2}{243(m_S + m_X)^4} + \frac{64m_S^2}{243(2m_X - m_S)^4} + \frac{176}{9m_S^2} - \frac{371m_S}{8m_X^3} \right. \\ &- \frac{15619}{36m_S m_X} + \frac{1387627}{26244m_S(m_S + m_X)} - \frac{6586685}{6561m_S(2m_X - m_S)} + \frac{15541}{9m_S(m_S + 2m_X)} \\ &+ \frac{528025}{34992(m_S + m_X)^2} + \frac{408049}{2187(2m_X - m_S)^2} + \frac{3707}{9(m_S + 2m_X)^2} + \frac{1961m_S}{729(m_S + m_X)^3} \\ &\left. - \frac{8656m_S}{729(2m_X - m_S)^3} + \frac{8529}{16m_X^2} \right), \end{aligned} \quad (C4)$$

$$\begin{aligned} \langle \sigma v^2 \rangle_{XSS \rightarrow XS} &\simeq \frac{[3(2m_X + m_S)(2m_X + 3m_S)]^{1/2}}{128\pi m_X^3 m_S(m_X + 2m_S)^2} 2\lambda_X^6 m_X^2 \\ &\left( \frac{6075m_S^2}{16m_X^4} + \frac{48(78m_S + 59m_X)}{m_S(-m_S^2 + 2m_S m_X + 2m_X^2)} + \frac{32(16m_S^2 + 11m_S m_X)}{(-m_S^2 + 2m_S m_X + 2m_X^2)^2} \right. \\ &+ \frac{36m_S^2}{(m_S + m_X)^4} + \frac{36m_S^2}{(m_S + 2m_X)^4} - \frac{4887m_S}{4m_X^3} - \frac{65425}{16m_S m_X} + \frac{10925}{4m_S(m_S + m_X)} \\ &+ \frac{583}{48m_S(2m_S + m_X)} - \frac{422}{3m_S(m_S + 2m_X)} + \frac{3935}{4(m_S + m_X)^2} + \frac{551}{24(2m_S + m_X)^2} \\ &\left. + \frac{851}{12(m_S + 2m_X)^2} + \frac{234m_S}{(m_S + m_X)^3} - \frac{394m_S}{(m_S + 2m_X)^3} + \frac{1245}{m_X^2} \right), \end{aligned} \quad (C5)$$

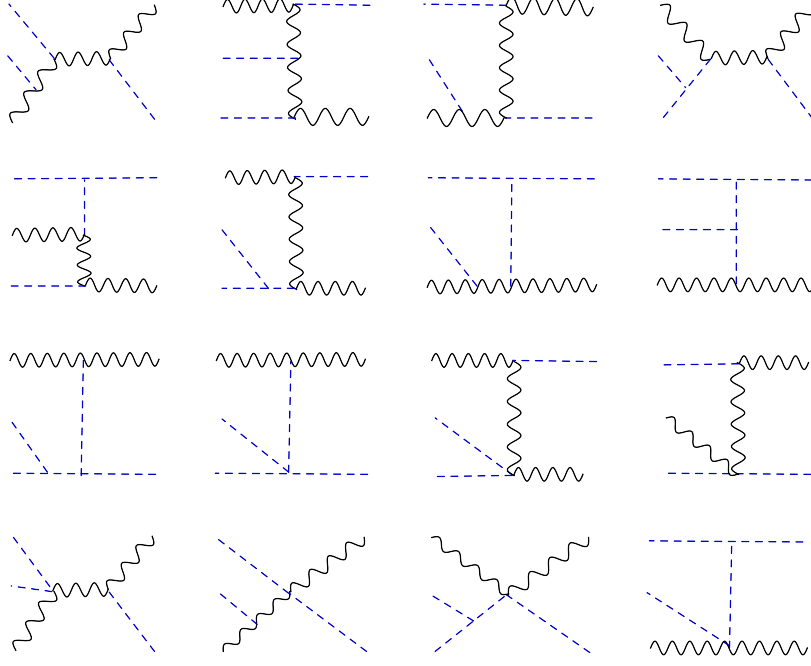
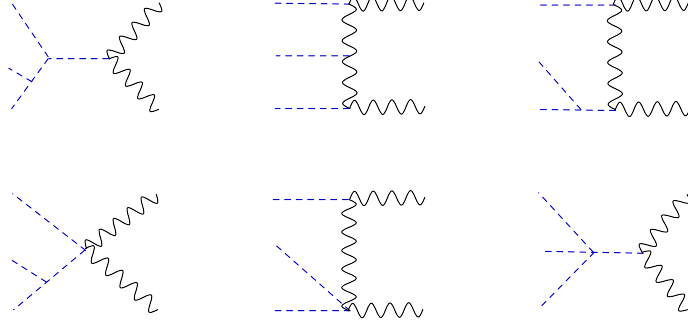
FIG. 10. Feynman diagrams for the annihilation  $XXX \rightarrow XS$ .FIG. 11. Feynman diagrams for the annihilation  $XXS \rightarrow SS$ .

$$\langle \sigma v^2 \rangle_{SSS \rightarrow XX} \simeq \frac{\sqrt{9 - 4m_X^2/m_S^2}}{384\pi m_S^3 m_X^2} \lambda_X^6 m_X^2 \times \left( \frac{432m_X^6}{m_S^8} - \frac{2160m_X^4}{m_S^6} + \frac{729m_S^4}{16m_X^6} + \frac{3672m_X^2}{m_S^4} + \frac{891m_S^2}{4m_X^4} - \frac{1944}{m_S^2} - \frac{729}{4m_X^2} \right), \quad (\text{C6})$$

$$\langle \sigma v^2 \rangle_{SSS \rightarrow SS} \simeq \frac{\sqrt{5}}{384\pi} \frac{18225}{16m_S^5} \left( \frac{\lambda_X m_S}{m_X} \right)^6. \quad (\text{C7})$$

#### Appendix D: The kinetic decoupling of the DM from the hidden scalar

In this Appendix, we discuss the epoch that the DM and hidden scalar starts to be kinetically decoupled from each other. For this period of time, which is well after  $3 \rightarrow 2$  annihilation

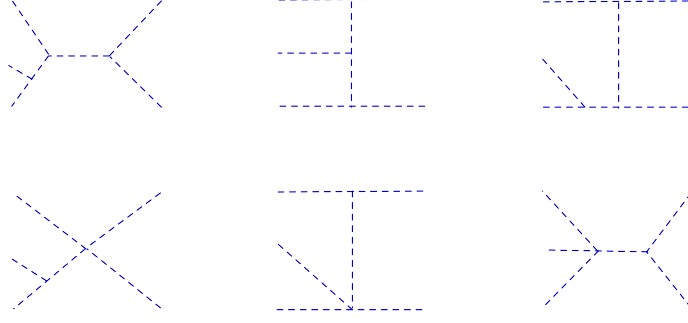
FIG. 12. Feynman diagrams for the annihilation  $XSS \rightarrow XS$ .FIG. 13. Feynman diagrams for the annihilation  $SSS \rightarrow XX$ .

decoupling, the DM temperature follows the Boltzmann equation,

$$\frac{dT_X}{dt} + 2HT_X \simeq -2\gamma_X(T_X - T_S) + \langle \sigma v \rangle_{XX \rightarrow SS}(T_S) \frac{(n_X^{\text{eq}}(T_S))^2}{(n_S^{\text{eq}}(T_S))^2} \frac{(n_S(T_S))^2}{n_X(T_X)} (T_S - T_X), \quad (\text{D1})$$

where the  $XS \rightarrow XS$  momentum relaxation rate is given by

$$\begin{aligned} \gamma_X(T_S) &= \frac{1}{768\pi^3 m_X^3 T_S} \int_0^\infty dE_S f_S(T_S) (1 + f_S(T_S)) \int_{-4\mathbf{p}_S^2}^0 dt (-t) |M_{XS \rightarrow XS}|^2 \\ &\simeq |M_{XS \rightarrow XS}|_{t=0}^2 \frac{1}{s=m_X^2+2m_X m_S} \frac{m_S^2}{12 m_X} \frac{T_S^2}{m_X^2} \left( 1 + 3 \frac{T_S}{m_S} + 3 \frac{T_S^2}{m_S^2} \right) e^{-m_S/T_S}. \end{aligned} \quad (\text{D2})$$

FIG. 14. Feynman diagrams for the annihilation  $SSS \rightarrow SS$ .

Based on the fact that  $-t \ll 4|\mathbf{p}|^2 \sim T \ll m_X^2, m_S^2$ , we neglect  $t$  in the calculation of the amplitude squared to obtain the approximate form of  $\gamma_X$ . Thus, the elastic scattering amplitude squared and summed over all internal degrees of freedom of initial and final spin states is given by

$$\begin{aligned}
 |M_{XS \rightarrow XS}|^2 &\simeq |M_{XS \rightarrow XS}|_{t=0}^2 \\
 &\quad s=m_X^2+2m_X m_S \\
 &\simeq 4\lambda_X^2 \cos^2 \alpha \left( \frac{3g_{SSS}^2 m_X^2}{m_S^4} + \frac{2\lambda_X g_{SSS} \cos \alpha m_X (4m_X^2 - 7m_S^2)}{m_S^2 (4m_X^2 - m_S^2)} \right. \\
 &\quad \left. + \frac{\lambda_X^2 \cos^2 \alpha (-32m_X^6 + 72m_X^4 m_S^2 - 56m_X^2 m_S^4 + 19m_S^6)}{m_S^2 (4m_X^2 - m_S^2)^2} \right). \quad (D3)
 \end{aligned}$$

Here the elastic scattering process  $XS \rightarrow XS$  contains the amplitudes with a hidden scalar  $S$  mediated in the  $t$ -channel and with  $X$  in the  $s/u$ -channel, and dominated by the former one. We define the DM kinetic decoupling temperature  $T_X^{\text{kd}}$  below which the kinetic energy injection rate transferred by the elastic scattering  $XS \rightarrow XS$  and/or by the annihilation  $SS \rightarrow XX$  to the DM falls below the diluting rate arising from the Hubble expansion.  $T_X^{\text{kd}}$  approximately satisfies

$$2\gamma_X(T_S) n_X(T_X) T_S + \langle \sigma v \rangle_{XX \rightarrow SS}(T_S) \frac{(n_X^{\text{eq}}(T_S))^2}{(n_S^{\text{eq}}(T_S))^2} (n_S(T_S))^2 T_S \simeq 2H(T) n_X(T_X) T_X, \quad (D4)$$

where, before kinetic decoupling,  $T_X = T_S$  are functions of  $T$  and can be determined from solving the Boltzmann moment equations. The results are shown in Figs. 3 and 4. The DM temperature after kinetic decoupling follows  $T_X(a) \simeq T_X^{\text{kd}} \cdot (a_X^{\text{kd}}/a)^2$ , with  $a$  being the cosmic scale factor and  $a_X^{\text{kd}}$  being the corresponding value at  $T_X^{\text{kd}}$ .

Similarly, if we consider the temperature below that the DM and hidden scalar are decoupled, the following two terms need to be included in the RHS of Eq. (44), which is the temperature evolution equation of  $S$ ,

$$-2\gamma_S(T_S - T_X) + \langle \sigma v \rangle_{XX \rightarrow SS}(T_X) \frac{(n_X(T_X))^2}{n_S(T_S)} (T_X - T_S), \quad (D5)$$

where the  $XS \rightarrow XS$  momentum relaxation rate is given by

$$\begin{aligned} \gamma_S(T_X) \simeq & \frac{1}{3} \frac{m_X^4}{m_S^3} \lambda_X^2 \cos^2 \alpha \left( \frac{3g_{SSS}^2 m_X^2}{m_S^4} + \frac{2\lambda_X g_{SSS} \cos \alpha m_X (4m_X^2 - 7m_S^2)}{m_S^2 (4m_X^2 - m_S^2)} \right. \\ & \left. + \frac{\lambda_X^2 \cos^2 \alpha (-32m_X^6 + 72m_X^4 m_S^2 - 56m_X^2 m_S^4 + 19m_S^6)}{m_S^2 (4m_X^2 - m_S^2)^2} \right) \frac{T_X^2}{m_X^2} \left( 1 + 3 \frac{T_X}{m_X} + 3 \frac{T_X^2}{m_X^2} \right) e^{-m_X/T_X} . \end{aligned} \quad (\text{D6})$$

- 
- [1] L. Goodenough and D. Hooper, “Possible Evidence For Dark Matter Annihilation In The Inner Milky Way From The Fermi Gamma Ray Space Telescope,” arXiv:0910.2998 [hep-ph].
  - [2] D. Hooper and L. Goodenough, “Dark Matter Annihilation in The Galactic Center As Seen by the Fermi Gamma Ray Space Telescope,” Phys. Lett. B **697**, 412 (2011) [arXiv:1010.2752 [hep-ph]].
  - [3] D. Hooper and T. Linden, “On The Origin Of The Gamma Rays From The Galactic Center,” Phys. Rev. D **84**, 123005 (2011) [arXiv:1110.0006 [astro-ph.HE]].
  - [4] K. N. Abazajian and M. Kaplinghat, “Detection of a Gamma-Ray Source in the Galactic Center Consistent with Extended Emission from Dark Matter Annihilation and Concentrated Astrophysical Emission,” Phys. Rev. D **86**, 083511 (2012) Erratum: [Phys. Rev. D **87**, 129902 (2013)] [arXiv:1207.6047 [astro-ph.HE]].
  - [5] C. Gordon and O. Macias, “Dark Matter and Pulsar Model Constraints from Galactic Center Fermi-LAT Gamma Ray Observations,” Phys. Rev. D **88**, no. 8, 083521 (2013) Erratum: [Phys. Rev. D **89**, no. 4, 049901 (2014)] [arXiv:1306.5725 [astro-ph.HE]].
  - [6] W. C. Huang, A. Urbano and W. Xue, “Fermi Bubbles under Dark Matter Scrutiny. Part I: Astrophysical Analysis,” arXiv:1307.6862 [hep-ph].
  - [7] T. Daylan, D. P. Finkbeiner, D. Hooper, T. Linden, S. K. N. Portillo, N. L. Rodd and T. R. Slatyer, “The characterization of the gamma-ray signal from the central Milky Way: A case for annihilating dark matter,” Phys. Dark Univ. **12**, 1 (2016) [arXiv:1402.6703 [astro-ph.HE]].
  - [8] F. Calore, I. Cholis and C. Weniger, “Background model systematics for the Fermi GeV excess,” JCAP **1503**, 038 (2015) [arXiv:1409.0042 [astro-ph.CO]].
  - [9] F. Calore, I. Cholis, C. McCabe and C. Weniger, “A Tale of Tails: Dark Matter Interpretations of the Fermi GeV Excess in Light of Background Model Systematics,” Phys. Rev. D **91**, no. 6, 063003 (2015) [arXiv:1411.4647 [hep-ph]].
  - [10] C. Karwin, S. Murgia, T. M. P. Tait, T. A. Porter and P. Tanedo, “Dark Matter Interpretation of the Fermi-LAT Observation Toward the Galactic Center,” Phys. Rev. D **95**, no. 10, 103005 (2017) [arXiv:1612.05687 [hep-ph]].
  - [11] M. Ackermann *et al.* [Fermi-LAT Collaboration], “The Fermi Galactic Center GeV Excess and Implications for Dark Matter,” Astrophys. J. **840**, no. 1, 43 (2017) [arXiv:1704.03910 [astro-ph.HE]].
  - [12] E. Aprile *et al.* [XENON Collaboration], “First Dark Matter Search Results from the XENON1T Experiment,” Phys. Rev. Lett. **119**, no. 18, 181301 (2017) [arXiv:1705.06655 [astro-ph.CO]].

- [13] X. Cui *et al.* [PandaX-II Collaboration], “Dark Matter Results From 54-Ton-Day Exposure of PandaX-II Experiment,” *Phys. Rev. Lett.* **119**, no. 18, 181302 (2017) [arXiv:1708.06917 [astro-ph.CO]].
- [14] D. S. Akerib *et al.* [LUX Collaboration], “Results from a search for dark matter in the complete LUX exposure,” *Phys. Rev. Lett.* **118**, no. 2, 021303 (2017) [arXiv:1608.07648 [astro-ph.CO]].
- [15] D. S. Akerib *et al.* [LUX-ZEPLIN Collaboration], “Projected WIMP Sensitivity of the LUX-ZEPLIN (LZ) Dark Matter Experiment,” arXiv:1802.06039 [astro-ph.IM].
- [16] M. Pospelov, A. Ritz and M. B. Voloshin, “Secluded WIMP Dark Matter,” *Phys. Lett. B* **662**, 53 (2008) [arXiv:0711.4866 [hep-ph]].
- [17] P. Ko, W. I. Park and Y. Tang, “Higgs portal vector dark matter for GeV scale  $\gamma$ -ray excess from galactic center,” *JCAP* **1409**, 013 (2014) [arXiv:1404.5257 [hep-ph]].
- [18] A. Berlin, P. Gratia, D. Hooper and S. D. McDermott, “Hidden Sector Dark Matter Models for the Galactic Center Gamma-Ray Excess,” *Phys. Rev. D* **90**, no. 1, 015032 (2014) [arXiv:1405.5204 [hep-ph]].
- [19] M. Escudero, S. J. Witte and D. Hooper, “Hidden Sector Dark Matter and the Galactic Center Gamma-Ray Excess: A Closer Look,” *JCAP* **1711**, no. 11, 042 (2017) [arXiv:1709.07002 [hep-ph]].
- [20] P. Ko and Y. Tang, “Galactic center  $\gamma$ -ray excess in hidden sector DM models with dark gauge symmetries: local  $Z_3$  symmetry as an example,” *JCAP* **1501**, 023 (2015) [arXiv:1407.5492 [hep-ph]].
- [21] M. Abdullah, A. DiFranzo, A. Rajaraman, T. M. P. Tait, P. Tanedo and A. M. Wijangco, “Hidden on-shell mediators for the Galactic Center  $\gamma$ -ray excess,” *Phys. Rev. D* **90**, 035004 (2014) [arXiv:1404.6528 [hep-ph]].
- [22] A. Martin, J. Shelton and J. Unwin, “Fitting the Galactic Center Gamma-Ray Excess with Cascade Annihilations,” *Phys. Rev. D* **90**, no. 10, 103513 (2014) [arXiv:1405.0272 [hep-ph]].
- [23] Y. G. Kim, K. Y. Lee, C. B. Park and S. Shin, “Secluded singlet fermionic dark matter driven by the Fermi gamma-ray excess,” *Phys. Rev. D* **93**, no. 7, 075023 (2016) [arXiv:1601.05089 [hep-ph]].
- [24] K. C. Yang, “Search for Scalar Dark Matter via Pseudoscalar Portal Interactions: In Light of the Galactic Center Gamma-Ray Excess,” *Phys. Rev. D* **97**, no. 2, 023025 (2018) [arXiv:1711.03878 [hep-ph]].
- [25] S. Profumo, F. S. Queiroz, J. Silk and C. Siqueira, “Searching for Secluded Dark Matter with H.E.S.S., Fermi-LAT, and Planck,” *JCAP* **1803**, no. 03, 010 (2018) [arXiv:1711.03133 [hep-ph]].
- [26] P. A. R. Ade *et al.* [Planck Collaboration], “Planck 2015 results. XIII. Cosmological parameters,” *Astron. Astrophys.* **594**, A13 (2016) [arXiv:1502.01589 [astro-ph.CO]].
- [27] J. A. Dror, E. Kuflik and W. H. Ng, “Codecaying Dark Matter,” *Phys. Rev. Lett.* **117**, no. 21, 211801 (2016) [arXiv:1607.03110 [hep-ph]].
- [28] D. Pappadopulo, J. T. Ruderman and G. Trevisan, “Dark matter freeze-out in a nonrelativistic sector,” *Phys. Rev. D* **94**, no. 3, 035005 (2016) [arXiv:1602.04219 [hep-ph]].
- [29] M. Farina, D. Pappadopulo, J. T. Ruderman and G. Trevisan, “Phases of Cannibal Dark Matter,” *JHEP* **1612**, 039 (2016) [arXiv:1607.03108 [hep-ph]].

- [30] A. Berlin, D. Hooper and G. Krnjaic, “Thermal Dark Matter From A Highly Decoupled Sector,” *Phys. Rev. D* **94**, no. 9, 095019 (2016) [arXiv:1609.02555 [hep-ph]].
- [31] K. C. Yang, “Hidden Higgs portal vector dark matter for the Galactic center gamma-ray excess from the two-step cascade annihilation, and muon  $g - 2$ ,” *JHEP* **1808**, 099 (2018) [arXiv:1806.05663 [hep-ph]].
- [32] Y. Hochberg, E. Kuflik, T. Volansky and J. G. Wacker, “Mechanism for Thermal Relic Dark Matter of Strongly Interacting Massive Particles,” *Phys. Rev. Lett.* **113**, 171301 (2014) [arXiv:1402.5143 [hep-ph]].
- [33] E. Kuflik, M. Perelstein, N. R. L. Lorier and Y. D. Tsai, “Elastically Decoupling Dark Matter,” *Phys. Rev. Lett.* **116**, no. 22, 221302 (2016) [arXiv:1512.04545 [hep-ph]].
- [34] E. Kuflik, M. Perelstein, N. R. L. Lorier and Y. D. Tsai, “Phenomenology of ELDER Dark Matter,” *JHEP* **1708**, 078 (2017) [arXiv:1706.05381 [hep-ph]].
- [35] M. Tanabashi et al. (Particle Data Group), *Phys. Rev. D* **98**, 030001 (2018).
- [36] J. M. Cline, K. Kainulainen, P. Scott and C. Weniger, “Update on scalar singlet dark matter,” *Phys. Rev. D* **88**, 055025 (2013) Erratum: [*Phys. Rev. D* **92**, no. 3, 039906 (2015)] [arXiv:1306.4710 [hep-ph]].
- [37] P. A. R. Ade *et al.* [Planck Collaboration], “Planck 2013 results. XVI. Cosmological parameters,” *Astron. Astrophys.* **571**, A16 (2014) [arXiv:1303.5076 [astro-ph.CO]].
- [38] T. Bringmann and S. Hofmann, “Thermal decoupling of WIMPs from first principles,” *JCAP* **0704**, 016 (2007) Erratum: [*JCAP* **1603**, no. 03, E02 (2016)] [hep-ph/0612238].
- [39] T. Bringmann, “Particle Models and the Small-Scale Structure of Dark Matter,” *New J. Phys.* **11**, 105027 (2009) [arXiv:0903.0189 [astro-ph.CO]].
- [40] P. Gondolo, J. Hisano and K. Kadota, “The Effect of quark interactions on dark matter kinetic decoupling and the mass of the smallest dark halos,” *Phys. Rev. D* **86**, 083523 (2012) [arXiv:1205.1914 [hep-ph]].
- [41] L. Visinelli and P. Gondolo, “Kinetic decoupling of WIMPs: analytic expressions,” *Phys. Rev. D* **91**, no. 8, 083526 (2015) [arXiv:1501.02233 [astro-ph.CO]].
- [42] T. Binder, L. Covi, A. Kamada, H. Murayama, T. Takahashi and N. Yoshida, “Matter Power Spectrum in Hidden Neutrino Interacting Dark Matter Models: A Closer Look at the Collision Term,” *JCAP* **1611**, 043 (2016) [arXiv:1602.07624 [hep-ph]].
- [43] T. Binder, T. Bringmann, M. Gustafsson and A. Hryczuk, “Early kinetic decoupling of dark matter: when the standard way of calculating the thermal relic density fails,” *Phys. Rev. D* **96**, no. 11, 115010 (2017) [arXiv:1706.07433 [astro-ph.CO]].
- [44] J. F. Navarro, C. S. Frenk and S. D. M. White, “The Structure of cold dark matter halos,” *Astrophys. J.* **462**, 563 (1996) [astro-ph/9508025].
- [45] J. F. Navarro, C. S. Frenk and S. D. M. White, “A Universal density profile from hierarchical clustering,” *Astrophys. J.* **490**, 493 (1997) [astro-ph/9611107].
- [46] G. Elor, N. L. Rodd and T. R. Slatyer, “Multistep cascade annihilations of dark matter and the Galactic Center excess,” *Phys. Rev. D* **91**, 103531 (2015) [arXiv:1503.01773 [hep-ph]].



- [47] M. Cirelli *et al.*, “PPPC 4 DM ID: A Poor Particle Physicist Cookbook for Dark Matter Indirect Detection,” JCAP **1103**, 051 (2011) Erratum: [JCAP **1210**, E01 (2012)] [arXiv:1012.4515 [hep-ph]].
- [48] P. Ciafaloni, D. Comelli, A. Riotto, F. Sala, A. Strumia and A. Urbano, “Weak Corrections are Relevant for Dark Matter Indirect Detection,” JCAP **1103**, 019 (2011) [arXiv:1009.0224 [hep-ph]].
- [49] T. Linden, N. L. Rodd, B. R. Safdi and T. R. Slatyer, “High-energy tail of the Galactic Center gamma-ray excess,” Phys. Rev. D **94**, no. 10, 103013 (2016) [arXiv:1604.01026 [astro-ph.HE]].
- [50] A. Albert *et al.* [Fermi-LAT and DES Collaborations], “Searching for Dark Matter Annihilation in Recently Discovered Milky Way Satellites with Fermi-LAT,” Astrophys. J. **834**, no. 2, 110 (2017) [arXiv:1611.03184 [astro-ph.HE]].
- [51] The data is available from the website: “[http://www-glast.stanford.edu/pub\\_data/1203/](http://www-glast.stanford.edu/pub_data/1203/)”.
- [52] T. R. Slatyer, “Indirect dark matter signatures in the cosmic dark ages. I. Generalizing the bound on s-wave dark matter annihilation from Planck results,” Phys. Rev. D **93**, no. 2, 023527 (2016) [arXiv:1506.03811 [hep-ph]].
- [53] M. Kawasaki, K. Kohri and N. Sugiyama, “MeV scale reheating temperature and thermalization of neutrino background,” Phys. Rev. D **62**, 023506 (2000) [astro-ph/0002127].
- [54] A. Djouadi, “The Anatomy of electro-weak symmetry breaking. II. The Higgs bosons in the minimal supersymmetric model,” Phys. Rept. **459**, 1 (2008) [hep-ph/0503173].
- [55] W. Y. Keung and W. J. Marciano, “Higgs Scalar Decays:  $H \rightarrow W^\pm X$ ,” Phys. Rev. D **30**, 248 (1984).
- [56] A. Djouadi, “The Anatomy of electro-weak symmetry breaking. I: The Higgs boson in the standard model,” Phys. Rept. **457**, 1 (2008) [hep-ph/0503172].
- [57] P. Gondolo and G. Gelmini, “Cosmic abundances of stable particles: Improved analysis,” Nucl. Phys. B **360**, 145 (1991).